ABSTRACT

ZHOU, QIAN. Thermophysical Properties of Ionic Liquid–LiX Mixtures. (Under the direction of Wesley A. Henderson.)

Ionic liquids (ILs) have attracted strong interest due to their high chemical, thermal and electrochemical stability; wide liquid range; high ionic conductivity and low volatility. The research objective of this project has been to explore the thermophysical properties of ILs and their mixtures with lithium salts (LiX). These mixtures may become the electrolyte materials essential for the success of safer, high-voltage next-generation lithium batteries targeted for plug-in hybrid electric vehicles (PHEVs) and/or electric vehicles (EVs). At present, there is only a limited amount of data available in the literature regarding the thermal stability and phase behavior of IL-LiX electrolytes. Such information, however, is crucial for determining the electrolyte safety characteristics and useful operating temperature range, as well as for clarifying the composition-temperature relationship for other properties such as ionic conductivity. The thermal phase behavior, thermal stability and other properties (viscosity and density) are reported here for the neat ILs containing 1-alkyl-3-methylimidazolium (IM_{10R}^{+}, R = 1, 2 and 4 for methyl, ethyl and butyl, respectively) or *N*-alkyl-*N*-methylpyrrolidinium (PY_{1R}^{+}, R = 3-5) cations with $TFSI^{-}$ or FSI^{-} anions, as well as their mixtures with LiTFSI or LiFSI salts. Three components electrolytes (1-x) PY_{14}TFSI-(x) PY_{13}FSI-LiX mixtures (X = $TFSI^{-}$ and PF_6^{-}) have also been examined. Such electrolytes show great promise for meeting the strick demands in properties necessary to achieve the superb Li battery performance and longevity required for the successful widespread use of PHEVs and/or EVs.

© Copyright 2009 by Qian Zhou

All Rights Reserved

Thermophysical Properties of Ionic Liquid-LiX Mixtures

by
Qian Zhou

A thesis submitted to the Graduate Faculty of
North Carolina State University
in partial fulfillment of the
requirements for the Degree of
Master of Science

Chemical Engineering

Raleigh, North Carolina

2009

APPROVED BY:

Saad Khan

Michael Dickey

Wesley A. Henderson
Chair of Advisory Committee

BIOGRAPHY

Qian Zhou was born on January 19, 1983 in Sichuan Province, China. She spent her childhood with her grandparents in Shanxi Province, and then moved to Xi'an in 1989. After graduating from Northwestern Polytechnical University (NPU) Middle School in 2001, she attended Harbin Institute of Technology (HIT) for her undergraduate studies. She graduated with her Bachelors of Science in Applied Chemistry in July 2005 and then enrolled in a two year Master's Degree Program in Queen Mary, University of London (QMUL). In 2005, she was awarded a Merit Master Degree of Materials and Business and joined the Department of Chemical and Biomolecular Engineering at North Carolina State University (NCSU) as a graduate student in 2007.

ACKNOWLEDGMENTS

First and foremost, I would like to thank my advisor Dr. Wesley Henderson for his full support and great guidance. It is hard to count how many times I came into his office full of confusion or even frustration, but came out with excitement and confidence. I thank him for treating me not only as a member of the Ionic Liquids and Electrolytes for Energy Technologies (ILEET) laboratory, but also as a friend.

I would like to thank Drs. Saad Khan and Maurice Balik and their research groups for their assistance in the thermal phase behavior and stability testing with special thanks to Brad Busche, Christopher Bonino and Ali Evren Ozcam. I am indebted to them for supporting me and sharing with me their wisdom, insight and humor.

My many thanks go to present and former members of the ILEET laboratory: Kate Brown, Daniel Seo, Joshua Allen, Menglong Hu, Kendall Fitzgerald and Mattew Gebbie for helping me with the research. Additionally, I owe a special thanks to Drs. Xinglian Geng and Elie Paillard for sharing their research experience with me through many useful discussions.

Assistance received from all members of the research and technical staff in the Department of Chemical and Biomolecular Engineering at North Carolina State University is also gratefully acknowledged with special thanks to Sandra Bailey and Diane Harper.

I would like to thank my parents and grandparents for their unconditionally love and support. They have been there every step in my life and without them I would never have become the person that I am. I thank them every day of my life. Finally, I would like to give my deepest thanks to my husband Haibo Zhao for his endless love, support and encouragement.

TABLE OF CONTENTS

LIST OF TABLES..... v
LIST OF FIGURES..... vi

1 Introduction..... 1
1.1 Li-Ion Batteries ─ Chemistry and Applications..... 1
1.1.1 Lithium Batteries..... 1
1.1.2 Lithium-Ion Battery..... 3
1.2 Electrolyte Materials..... 5
1.2.1 State-of-the-Art Liquid Electrolytes..... 6
1.2.2 Lithium Salts..... 7
1.2.3 Solvent Selection..... 8
1.3 Properties of Ionic Liquids..... 12
1.3.1 Ionic Liquids..... 12
1.3.2 Future Li-Ion Batteries and Ionic Liquids..... 13
References..... 14
2 Experimental Procedures..... 18
2.1 Materials 18
2.2 Sample Preparation..... 18
2.3 Instruments and Techniques..... 20
References..... 23
3 Ionic Liquids (ILs) 24
3.1 Introduction..... 24
3.2 $IM_{10R}TFSI$ (R = 1, 2 and 4) ILs..... 25
3.3 $PY_{1R}TFSI$ (R = 3-5) ILs..... 29
3.4 $PY_{1R}FSI$ (R = 3 and 4) ILs..... 31
References..... 35
4 Ionic Liquid–Lithium Salt Electrolytes..... 39
4.1 Introduction..... 39
4.2 (1-x) $IM_{10R}TFSI$–(x) LiTFSI Mixtures..... 40
4.3 (1-x) $PY_{1R}TFSI$–(x) LiTFSI Mixtures..... 46
4.4 (1-x) $PY_{14}FSI$–(x) LiFSI Mixtures..... 48
4.5 Discussion..... 50
References..... 51
5 Ionic Liquid(1)–Ionic Liquid(2)–Lithium Salt Electrolytes..... 53
5.1 Introduction..... 53
5.2 (1-x) $PY_{14}TFSI$-(x) $PY_{13}FSI$-0.3M LiX Mixtures (X = $TFSI^-$ or PF_6^-)..... 54
5.3 Discussion..... 57
References..... 58

LIST OF TABLES

Table 1-1 Advantages and disadvantages of Li-ion batteries[1]..... 4

Table 1-2 Structure of aprotic solvents of potential interest for Li-ion batteries..... 9

Table 1-3 Physical property data of select solvents..... 11

Table 1-4 Examples of IL cation structures (1,3-dialkylimidazolium, 1,2,3-trialkylimidazolium, tetraalkylammonium, *N*,*N*-dialkylpyrrolidinium, *N*,*N*-dialkylpip-eridinium and *N*,*N*-dialkylmorpholinium)..... 12

Table 2-1 ^{1}H NMR data for $IM_{10R}TFSI$ (R = 1, 2 and 4) and $PY_{1R}TFSI$ (R = 3-5), δ_H (200 MHz, CD_3CN)..... 20

Table 5-1 Mole composition of (1-x) $PY_{14}TFSI$-(x) $PY_{13}FSI$-0.3M LiX mixtures (X = $TFSI^-$ or PF_6^-). The parameters x and (1-x) are the mole fractions of $PY_{13}FSI$ and $PY_{14}TFSI$, respectively..... 53

LIST OF FIGURES

Fig. 1-1. Schematic of the components of a Li metal battery..... 1
Fig. 1-2. Schematic description for: (a) the growth of dendrite crystals on a Li surface during recharging resulting in the formation of treelike dendrites and (b) the formation of isolated Li particles from Li dendrites[11]..... 1
Fig. 1-3. Typical SEM micrographs of single dendrites formed by lithium deposition: (a) PC-0.5M $LiClO_4$ solution and (b) BL-0.5M $LiClO_4$ solution[12]..... 2
Fig. 1-4. Electrode and cell reactions in a Li-ion cell..... 3
Fig. 1-5. Resonance structures of the $TFSI^-$..... 7
Fig. 1-6. Variable-temperature TGA traces (5°C min^{-1}) of LiTFSI (N_2 atmosphere)... 8
Fig. 2-1. Synthesis procedure for the $PY_{1R}TFSI$ ILs..... 18
Fig. 2-2. ^1H NMR spectrum for CD_3CN..... 20
Fig. 2-3. ^1H NMR spectrum for $IM_{10R}TFSI$ (R = 1, 2 and 4) and $PY_{1R}TFSI$ (R = 3-5), δ_H (200 MHz, CD_3CN)..... 21
Fig. 3-1. Chemical structures of IM_{10R}^+ (R = 1, 2 and 4) and PY_{1R}^+ (R = 3-5) cations and $TFSI^-$ and FSI^- anions..... 24
Fig. 3-2. DSC heating traces (5°C min^{-1}) of $IM_{102}TFSI$: (a)-(c) are for different thermal histories (see text)..... 25
Fig. 3-3. $TFSI^-$ anion conformations. (a) C_1 conformer and (b) C_2 conformer (two views of each shown)..... 26
Fig. 3-4. Variable-temperature TGA traces (5°C min^{-1}) of $IM_{10R}TFSI$ (N_2 atmosphere)..... 26
Fig. 3-5. Isothermal TGA traces of (a) $IM_{101}TFSI$, (b) $IM_{102}TFSI$ and (c) $IM_{104}TFSI$ (N_2 atmosphere). The temperature for each measurement is indicated in the figure..... 27
Fig. 3-6. Variable-temperature (a) viscosity and (b) density of $IM_{10R}TFSI$ (R = 2,4).. 28
Fig. 3-7. DSC heating traces (5°C min^{-1}) of $PY_{1R}TFSI$ (R = 3-5)..... 29
Fig. 3-8. DSC heating traces (10°C min^{-1}) of $PY_{14}TFSI$ after quenching (top) or slow cooling/annealing (bottom) from room temperature[1]..... 29
Fig. 3-9. Variable-temperature TGA traces (5°C min^{-1}) of $PY_{1R}TFSI$ (N_2 atmosphere)..... 29
Fig. 3-10. Variable-temperature (a) viscosity and (b) density of $PY_{1R}TFSI$ (R = 3-5)... 30
Fig. 3-11. DSC cooling and heating traces (5°C min^{-1}) of (a) $PY_{13}FSI$ and (b) $PY_{14}FSI$..... 31
Fig. 3-12. Variable-temperature TGA traces (5°C min^{-1}) of $PY_{1R}FSI$: (a) N_2 and (b) air atmosphere..... 32
Fig. 3-13. Isothermal TGA traces of $PY_{1R}FSI$: (a) R = 3 and (b) R = 4 (N_2 atmosphere). The temperature for each measurement is indicated in the figure..... 33
Fig. 3-14. Variable-temperature viscosity of $PY_{1R}FSI$ (R = 3,4)..... 34
Fig. 4-1. DSC heat traces (5°C min^{-1}) of (1-x) $IM_{10R}TFSI$-(x) LiTFSI mixtures: (a) R

= 1, (b) R = 2 and (c) R = 4 (peak and T_g temperatures are noted)…….. 41
Fig. 4-2. Portion of the crystal structure of the (1-x) $IM_{102}CF_3SO_3$-(x) $LiCF_3SO_3$ (x = 0.50) (or 1/1 $IM_{101}CF_3SO_3/LiCF_3SO_3$) crystalline phase (two views shown).[6] The C and N atoms of the IM_{102}^+ cations are colored black for clarity…… 41
Fig. 4-3. Portion of the crystal structure of the (1-x) IM_{102}TFSI-(x) LiTFSI (x = 0.67) (or 1/2 IM_{102}TFSI/ LiTFSI) crystalline phase (two views). The C and N atoms of the IM_{102}^+ cations are colored black and the two cations have been removed from the left cavity for clarity[8]…….. 42
Fig. 4-4. Variable-temperature TGA traces (5°C min^{-1}) of (1-x) IM_{10R}TFSI-(x) LiTFSI mixtures (N_2 atmosphere): (a) R = 2 and (b) R = 4; and mass remaining for (1-x) IM_{10R}TFSI-(x) LiTFSI mixtures after isothermal TGA runs (N_2 atmosphere), open circles for R = 2 and filled circles for R = 4: (c) 225°C and (d) 250°C…… 44
Fig. 4-5. Variable-temperature (a) viscosity and (b) density of (1-x) IM_{10R}TFSI-(x) LiTFSI mixtures (open symbols for R = 2 and filled symbols for R = 4)…… 46
Fig. 4-6. DSC heating traces (5°C min^{-1}) of (1-x) PY_{1R}TFSI-(x) LiTFSI mixtures: (a) R = 2, (b) R = 3 and (c) R = 4 (peak and T_g temperatures are noted)[3]……. 47
Fig. 4-7. DSC heating traces (5°C min^{-1}) of (1-x) PY_{14}FSI-(x) LiFSI (peak and T_g temperatures are noted)……. 48
Fig. 4-8. Variable temperature TGA traces (5°C min^{-1}) of (1-x) PY_{14}FSI-(x) LiFSI mixtures (N_2 atmosphere)……. 48
Fig. 4-9. Isothermal TGA traces for: (a) (1-x) PY_{14}FSI-(x) LiFSI (x = 0.10) (N_2 atmosphere). The temperature for each scan is indicated in the figure and (b) (1-x) PY_{14}FSI-(x) LiFSI mixtures at 100°C (N_2 atmosphere). Mole fraction is indicated in the figure……... 49
Fig. 4-10. Variable-temperature viscosity of (1-x) PY_{14}FSI-(x) LiFSI mixtures…… 50
Fig. 5-1. DSC heat traces (5°C min^{-1}) of (1-x) PY_{14}TFSI-(x) PY_{13}FSI-0.3M $LiPF_6$ (x = 1)…… 54
Fig. 5-2. DSC heat traces (5°C min^{-1}) of (1-x) PY_{14}TFSI-(x) PY_{13}FSI-0.3M LiX mixtures: (a) X = $TFSI^-$ and (b) X = PF_6^-……. 55
Fig. 5-3. Variable-temperature TGA traces (5°C min^{-1}) of (1-x) PY_{14}TFSI-(x) PY_{13}FSI-0.3M LiX mixtures: (a) X = $TFSI^-$ and (b) X = PF_6^- (N_2 atmosphere)……... 56
Fig. 5-4. Variable-temperature ionic conductivity of (1-x) PY_{14}TFSI-(x) PY_{13}FSI-0.3M LiX mixtures: (a) X = $TFSI^-$ and (b) X = PF_6^{-2}……... 58

Chapter 1. Introduction

1.1 Li-Ion Batteries: Chemistry and Applications

1.1.1 Lithium Batteries

Li metal is perhaps the optimal anode material for a battery as it combines a very high specific capacity (3.86 Ah g^{-1}, 7.23 Ah cm^{-3} due to its light weight) with a very favorable thermodynamic electrode potential enabling the formation of single-cell Li batteries (Fig. 1-1) with a potential in excess of 4 V.[1,2] Due to its electropositive nature, Li metal rapidly reduces water. In the 1950s, however, Li metal was found to be stable in nonaqueous solvents due to the formation of a passivation film on the Li surface.[3] This crucial discovery resulted in extensive research in the use of Li as a battery electrode in the following years.[4-7] Primary (non-rechargeable) cells which use Li metal as an anode are found to have numerous advantages as compared with other conventional batteries, such as a high

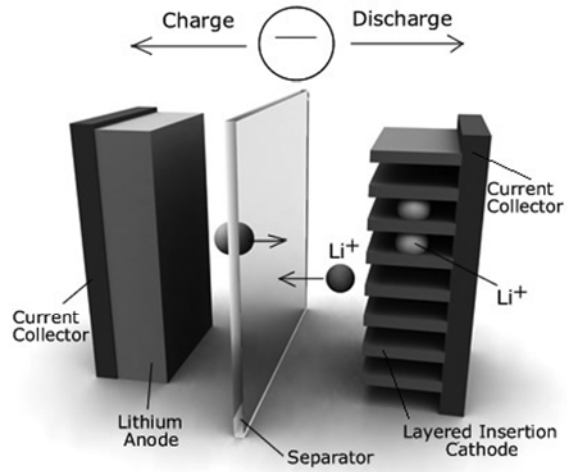

Fig. 1-1. Schematic of the components of a Li metal battery.

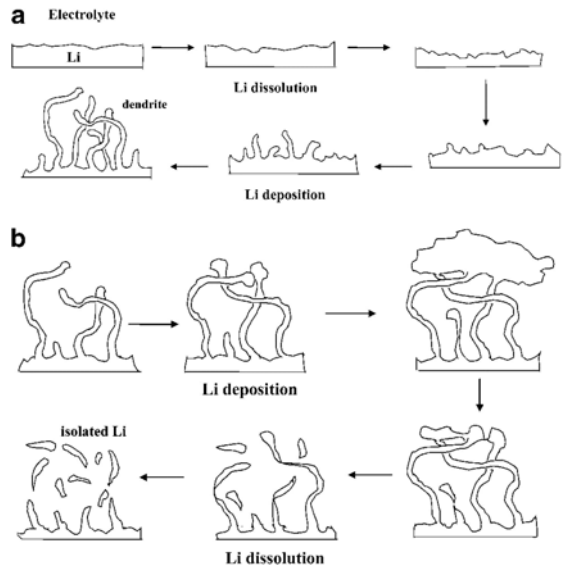

Fig. 1-2. Schematic description for: (a) the growth of dendrite crystals on a Li surface during recharging resulting in the formation of treelike dendrites and (b) the formation of isolated Li particles from Li dendrites.[11]

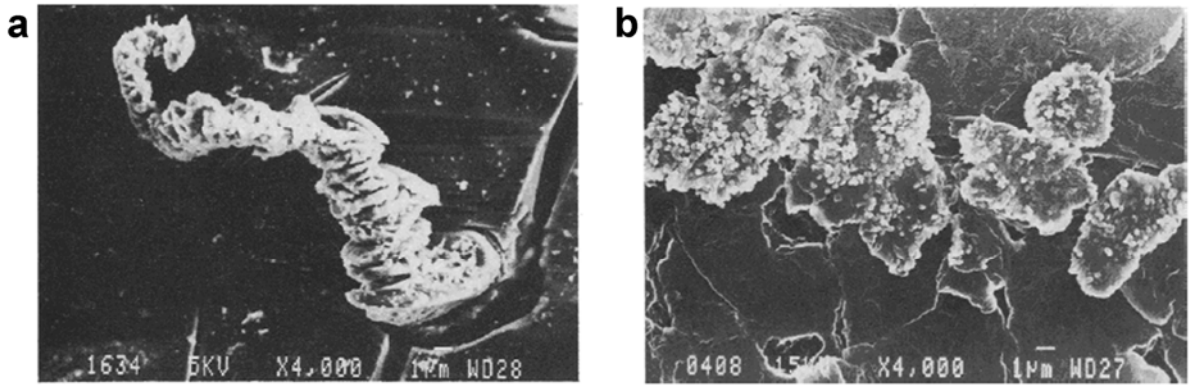

Fig. 1-3. Typical SEM micrographs of single dendrites formed by lithium deposition: (a) PC-0.5M $LiClO_4$ solution and (b) BL-0.5M $LiClO_4$ solution.[12]

voltage, high specific energy and energy density, wide operating temperature range, good power density, flat voltage discharge characteristics, superior shelf life, etc.[1,2]

For secondary (rechargeable) battery applications, however, a critical problem hindered the use of Li metal. A "dendritic" (needle-like Li crystals) structure was found to form on the Li anode when recharging the batteries (replating the Li metal).[8,9] This isolates the Li metal in the dendrites from the Li metal substrate during the subsequent discharge period (Fig. 1-2).[10] The nickname "dead lithium" was given to this phenomenon,[11] because this electrochemically inactive electrode material results in a significant energy density loss. A further complication is the possibility of the dendrites piercing the separator/electrolyte, thus contacting the cathode to create an internal short-circuit which may lead to thermal runaway (rapid heating produced from an uncontrolled battery reaction) and flamming of the battery or a battery explosion. SEM images of dendrite structure are shown in Fig. 1-3.[12] Due to such high risks, several producers of early commercial Li batteries recalled their batteries and research related to batteries which use Li metal as an anode was largely terminated in 1989.[13]

1.1.2 Lithium-Ion Battery

Due to the serious problems with rechargeable Li metal batteries, an alternative battery design based upon Li chemistry was proposed which was alternatively named "rocking-chair", "shuttle-cock" or "swing" batteries.[14-16] The term "lithium-ion or Li-ion" was finally adopted,[17-19] however, and this battery was introduced to the public in the late 1980s. In 1990, both Sony and Moli commercialized their first Li-ion battery[20-21] which rapidly became popular for consumer electronics applications, such as cell phones, laptop computers and personal data assistants, as well as military electronics, such as radios, mine detectors and thermal weapons sights. Large Li-ion batteries have also been increasingly used in space vehicles, satellites and electric or hybrid electric vehicles.[22]

The typical Li-ion battery consists of a carbonaceous (instead of Li metal) anode (typically graphite), a separator/electrolyte, a composite cathode containing a metal oxide active material (such as $LiCoO_2$, $LiMn_2O_4$ or $LiNiO_2$) and current collectors (Fig. 1-1 with the anode material replaced).[23] No Li metal is ever present in the battery. Rather, Li^+ cations are transported back and forth through the electrolyte between the intercalation electrodes, thus avoiding the formation of dendrites during the plating of Li metal, leading to a significant improvement in safety. Fig. 1-4 shows the charge/discharge reactions in a typical Li-ion battery.[1] When the battery is being charged, the metal oxide cathode (positive material) is

$$\text{Positive:}\quad LiMO_2 \underset{\text{discharge}}{\overset{\text{charge}}{\rightleftharpoons}} Li_{1-x}MO_2 + xLi^+ + xe^-$$

$$\text{Negative:}\quad C + xLi^+ + xe^- \underset{\text{discharge}}{\overset{\text{charge}}{\rightleftharpoons}} Li_xC$$

$$\text{Overall:}\quad LiMO_2 + C \underset{\text{discharge}}{\overset{\text{charge}}{\rightleftharpoons}} Li_xC + Li_{1-x}MO_2$$

Fig. 1-4. Electrode and cell reactions in a Li-ion cell.

Table 1-1. Advantages and disadvantages of Li-ion batteries.[1]

Advantages	Disadvantages
Sealed cells; no maintenance required	Moderate initial cost
Long cycle life	Degrades at high temperature
Broad temperature range of operation	Need for protective circuitry
Long shelf life	Capacity loss or thermal runaway when overcharged
Rapid charge capability	Venting and possible thermal when crushed
High rate and high power discharge capability	Cylindrical designs typically offer lower power density than NiCd or NiMH
High coulombic and energy efficiency	
High specific energy and energy density	
No memory effect	

oxidized and the carbon anode (negative material) is reduced. The Li^+ cations are then deintercalated from the cathode and intercalated into the anode.[1] The reverse reaction occurs during battery discharing.

The general merits and drawbacks of Li-ion batteries are summarized in Table 1-1. Such batteries have both high specific energy (~150 Wh kg^{-1}) and energy density (~400 Wh L^{-1}), as well as a low self-discharge rate (2-8% per month), long cycle life (more than 1000 cycles), a broad temperature range of operation (-10°C to 50°C) and a large electrochemical window, making the Li-ion battery suitable for numerous applications. The main disadvantage of these batteries, as for Li metal batteries, is safety issues. Under standard usage conditions, the batteries perform well. But mechanical short circuits or internal short circuits (as occurred for the Dell computer batteries recalled in 2006) may result in localized heating. If the Li-ion battery is heated above a certain temperature (usually above 130-150°C), exothermic chemical reactions begin to occur between the electrodes and electrolyte, causing the temperature to rapidly increase, eventually resulting in thermal runaway.[24-27]

Heating above 50°C tends to degrade the battery, but does not necessarily lead to thermal runaway.

Several techniques to improve safety have been utilized including device safety features, as well as inherently safer battery materials. Examples of the former include safety vents and positive temperature coefficient (PTC) elements,[24] while safer materials include shutdown separators,[28] redox shuttle mechanisms and more oxidation-tolerant and less volatile/flammable electrolyte constituents.

1.2 Electrolyte Materials

Electrolytes in current use for Li-ion battery include four principal types: liquid, gel, polymer and ceramic electrolytes.[1] Liquid electrolytes consist of a lithium salt (LiX) and one or more organic solvents. The conductive portion of gel electrolytes are solutions of LiX salts and solvents which are mixed with a high molecular weight polymer, but for polymer electrolytes the ionic conductivity originates from directly dissolving the LiX salt in a high molecular weight polymer such as poly(ethylene oxide) (the polymer serves as the solvent). Polymer electrolytes are therefore liquid-free materials, whereas a liquid can be separated from a gel electrolyte upon the application of pressure to the material. Both such electrolytes tend to form flexible membranes. Ceramic electrolytes, in contrast, are rigid inorganic solid-state materials. No matter which type of electrolyte is used, however, the function of the electrolyte is the same – it serves as the medium to transfer Li^+ cations (but not electrons) between the cell electrodes.[10]

1.2.1 State-of-the-Art Liquid Electrolytes

State-of-the-art liquid electrolytes used in most commercial Li-ion batteries consist of $LiPF_6$ dissolved in a mixture of ethylene carbonate (EC) and a linear carbonate (i.e., diethyl carbonate (DEC)).[10] Such electrolytes have a high ionic conductivity (>10^{-3} S cm^{-1}) and high Li^+ cation transference number (~0.35) (the fraction of the total current due to Li^+ cations).[1] The $LiPF_6$ and EC react with the graphite anode surface to form a stable interface (a solid electrolyte interface or SEI) which prevents further electrolyte decomposition, but permits rapid Li^+ cation transport. In addition, $LiPF_6$ reacts with Al at high potentials to form a stable, insoluble layer. This is vital since Al is used almost universally as the cathode current collector in Li-ion batteries. The stable layer prevents further corrosion of the current collector. All of these properties are essential for a Li-ion battery to have excellent performance and a reasonable longevity.

These electrolyte compositions are not without their drawbacks. $LiPF_6$ is hygroscopic and produces hydrofluoric acid (HF) when exposed to water, thus requiring a very strict working and storage environment. Further, $LiPF_6$ has a relatively low thermal stability[29,30] and the reaction of $LiPF_6$ with the aprotic solvents at elevated temperature produces fluorinated toxic compounds.[31] In addition, the EC solvent is believed to lead to a rapid increase in the viscosity at subambient temperatures resulting in an effective operating temperature lower limit of about -10°C. The upper operating temperature limit is about 50°C due to the degradation of the SEI layer and reactivity of the $LiPF_6$.

1.2.2 Lithium Salts

Other LiX salts, such as $LiBF_4$, $LiClO_4$, $LiAsF_6$, $LiCF_3SO_3$ and $LiN(SO_2CF_3)_2$ (or LiTFSI), have been examined as possible replacements for $LiPF_6$ in Li-ion battery applications.

Each of these suffers from problems which have precluded their use in rechargeable Li-ion batteries thus far. The bis(trifluoromethanesulfonyl)imide anion (as $HN(SO_2CF_3)_2$ or HTFSI) was first reported by Foropoulos and DesMarteau in 1984.[32] In the early 1990s, 3M commercialized LiTFSI.[10] The negative charge on the $TFSI^-$ anion is extensively delocalized due to resonance (Fig. 1-5) and the strong electron-withdrawing triflic groups. The melting point (T_m) of LiTFSI is 236°C, but the salt has been reported to not decompose until 360°C.[33]

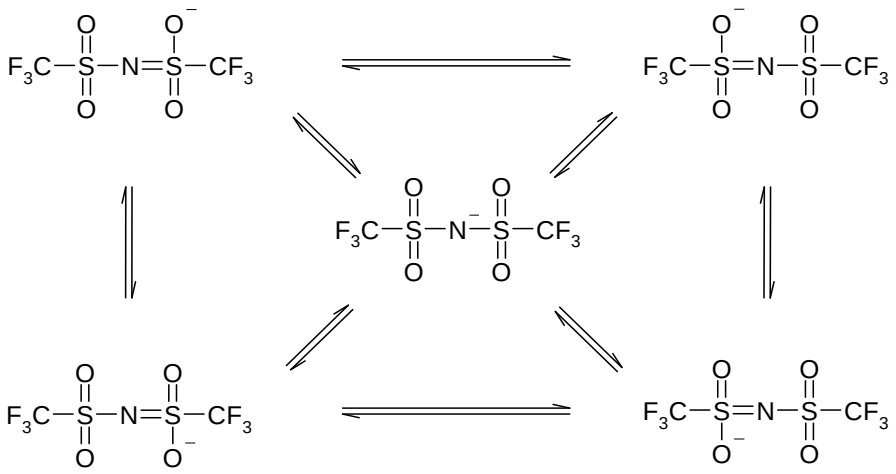

Fig. 1-5. Resonance structures of the $TFSI^-$.

Thermogravimetric studies of anhydrous LiTFSI were conducted in our lab and it was found that the onset point for mass loss (1 wt%) is around 327°C. Approximately 7 wt% of the original LiTFSI is left after heated to 600°C under an N_2 atmosphere (Fig. 1-6). An isothermal TGA study (not shown) indicates that LiTFSI loses approximately 1 wt% of its mass after heating at 250°C for 900 min. The main disadvantages associated with LiTFSI is its corrosion of Al. LiTFSI reacts with Al at high potentials to form $Al(TFSI)_3$, which is soluble in the aprotic solvents.[34] This solubility results in a fresh Al surface constantly exposed for continued corrosion reactions (in contrast with $LiPF_6$). Several methods have been suggested to solve this problem,[34-36] but this has not yet led to the use of LiTFSI in commercial Li-ion batteries.

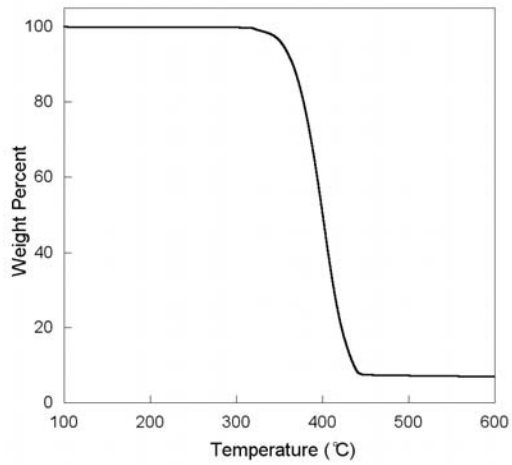

Fig. 1-6. Variable-temperature TGA traces (5°C min^{-1}) of LiTFSI (N_2 atmosphere).

1.2.3 Solvent Selection

Commercial liquid electrolytes utilize two (or more) solvents. Important properties of the electrolyte solvents include:[1]

- they must be aprotic (i.e., have no reactive protons);
- they must have low reactivity with graphite or other anode materials (or form a protective coating on the graphite surface to prevent further reaction) and the cathode;
- they must be capable of forming an electrolyte with a high ionic conductivity;
- they should form electrolyte solutions which are liquid over a broad temperature range;
- they should have favorable physical characteristics, such as low vapor pressure, high stability, nontoxicity and low flammability;

Table 1-2. Structure of aprotic solvents of potential interest for Li-ion batteries.

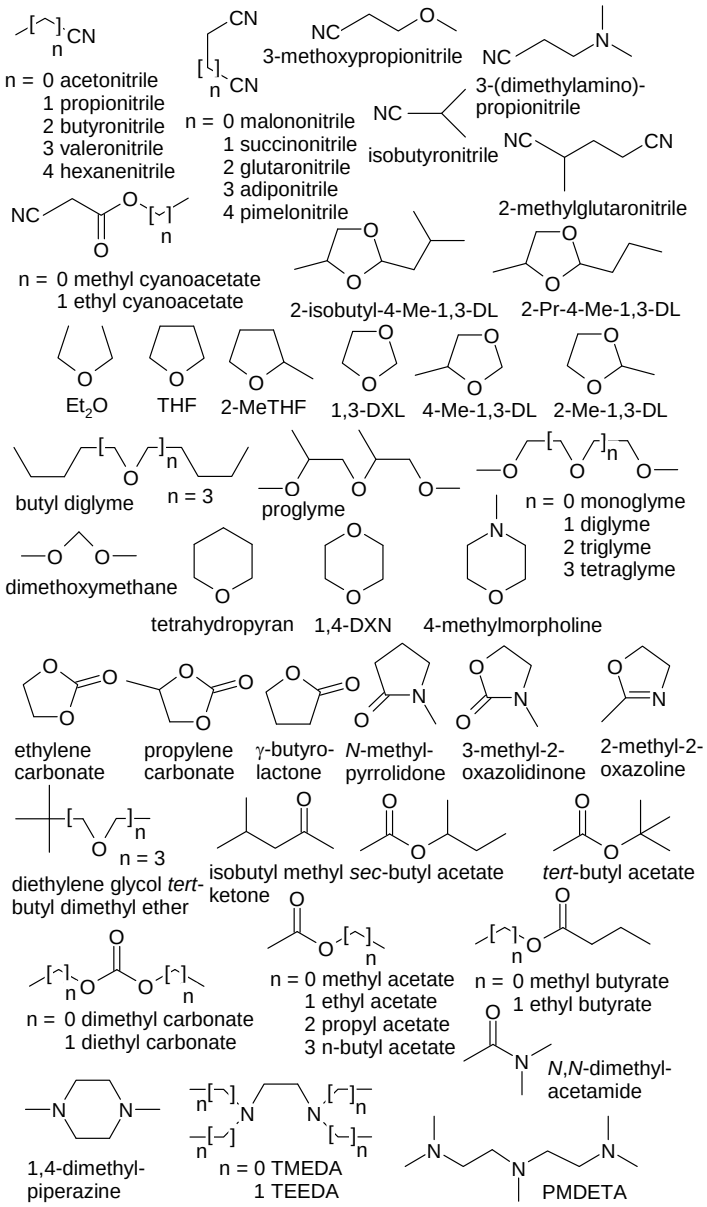

- they must be able to dissolve sufficient amounts of the LiX salt (typically a 1M concentration) and therefore contain polar functional groups such as one or more carbonyl, nitrile, sulfonyl, and/or ether groups.[10]

Table 1-2 shows the structures of some solvents of potential use for battery electrolytes. Carbonate solvents, such as EC, propylene carbonate (PC), dimethyl carbonate (DMC), ethyl methyl carbonate (EMC) and DEC, are currently the most widely used. Battery performance is enhanced by mixing two or more solvents together.[10] Single solvent-LiX mixtures tend not to have the properties necessary to meet the needs for battery applications. For example, EC has a high permittivity (and thus solvates Li^+ cations well), but the solvent is a solid at room temperature (T_m is 36°C).[10] Thus, a linear carbonate such as diethyl carbonate with a lower permittivity, but also with a low viscosity, is added to form a concentrated electrolyte solution with the LiX with low viscosity and high conductivity. Table 1-3 shows the physical properties of select solvents. Most aprotic organic solvents have a relatively low boiling point and are thus volatile as well as flammable.

Table 1-3. Physical property data of select solvents.

	f.p./m.p. (°C)	b.p. (°C)	flash pt. (°C)	ignition temp. (°C)	density[a] (g/mL)	viscosity[a] (cP)	vap. press.[a] (mm Hg)
acetonitrile	-45	82	2	524	0.786	0.34	73
propionitrile	-93	97	6		0.722		
butyronitrile	**-112**	**117**	**18**		**0.79**		**23**
valeronitrile	**-96**	**140**	**40**	**520**	**0.795**		**5.3**
hexanenitrile	-80	165	43		0.809		
malononitrile	30	220	86		1.049		
succinonitrile	53	266	113		0.985		< 2
glutaronitrile	-29	286	112		0.995		
adiponitrile	4	295	163	550	0.962		
pimelonitrile		>176	112		0.947		
3-methoxypropionitrile	**-62**	**165**	**66**	**390**	**0.939**		**1.72**
3-(dimethylamino)-propionitrile	-43	171	63		0.87		
methyl cyanoacetate	-13	87	113	505	1.127		0.2
ethyl cyanoacetate	-22	210	109		1.061		
2-methylglutaronitrile	-45	270	115		0.952		
isobutyronitrile	-72	108	8	250	0.770		
THF	-108	65	-14	321	0.889	0.46	129
2-MeTHF	-137	80	-11		0.85	0.47	
1,3-DL	-95	78	1		1.06	0.59	
4-Me-1,3-DL	-125	85	-2		0.983	0.60	
2-Me-1,3-DL		83	-2		0.982	0.54	
2-isobutyl-4-Me-1,3-DL		152	41		0.895		
2-Pr-4-Me-1,3-DL		137	32		0.906		
monoglyme (DME)	-69	85	0	200	0.868	1.1	48
diglyme	-64	162	57	190	0.945	2.0	3
triglyme	-45	216	111	195	0.986	3.8	
tetraglyme	-30	275	141	266	1.01		< 0.01
diethoxyethane	-74	121	20		0.84		
butyl diglyme	**-60**	**256**	**118**		**0.88**		
proglyme (dipropylene glycol dimethyl ether)	**-80**	**>280**	**149**	**215**	**1.04**	**12**	**< 0.01**
diethylene glycol *tert*-butyl ethyl ether		195-205			0.892		
N-methylpyrrolidone	-24	202	91	270	1.028		0.29
3-methyl-2-oxazolidinone	15	270	110		1.17	2.5	
ethylene carbonate	35	244	143		1.321		
propylene carbonate	**-55**	**242**	**132**	**455**	**1.189**		**0.13**
isobutyl methyl ketone	**-84**	**116**	**57**	**449**	**0.801**		**15**
***sec*-butyl acetate**	**-99**	**112**	**61**		**0.872**		
n-butyl acetate	-78	126	74		0.88		
dimethyl carbonate	5	91	18		1.063		
diethyl carbonate	**-74**	**126**	**31**		**0.969**		
ethyl acetate	**-84**	**77**			**0.902**		
methyl butyrate	-84	102			0.898		
ethyl butyrate	**-93**	**120**			**0.878**		

[a] At 20-25°C.

1.3 Properties of Ionic Liquids

1.3.1 Ionic Liquids

Ionic liquids (ILs) are salts or mixtures of salts (composed solely of ions) with a low melting temperature – often below room temperature.[37] ILs usually consist of asymmetric organic cations and inorganic anions. The most commonly used cations for ILs are imidazolium or aliphatic quaternary ammonium cations with various anions, such as halides [Cl, Br, I]$^-$, nitrate $[NO_3]^-$, acetate $[CH_3CO_2]^-$, tetrafluoroborate $[BF_4]^-$, triflate $[CF_3SO_3]^-$, hexafluorophoshate $[PF_6]^-$ and TFSI$^-$. Table 1-4 shows some examples of typical IL cations. ILs are considered to be "designer solvents" due to the ability to modify the physical and chemical properties of the salts by the selection of different cations, anions and alkyl side chain substituents (R groups).[38] Many ILs are liquids over a very broad temperature range (-80°C to 250°C or higher) with low or negligible vapor pressure; moreover, ILs may have low flammability, high thermal stability and high ionic conductivity.[39-42] ILs are therefore being extensively explored as replacements for conventional organic solvents in electrochemical, catalytical, synthetic and engineering processes due to their inherent safety, which significantly reduces the emissions of volatile organic compounds (VOCs) resulting in atmosphere pollution.[43,44]

Table 1-4. Examples of IL cation structures (1,3-dialkylimidazolium, 1,2,3-trialkylimidazolium, tetraalkylammonium, *N*,*N*-dialkylpyrrolidinium, *N*,*N*-dialkylpiperidinium and *N*,*N*-dialkylmorpholinium).

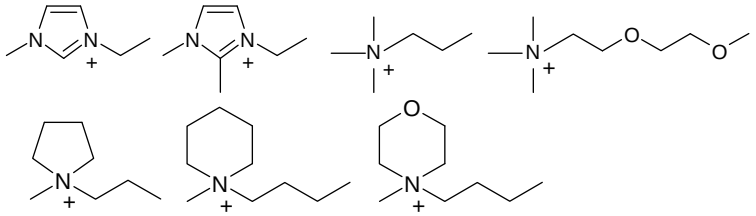

1.3.2 Future Li-Ion Batteries and Ionic Liquids

The unique characteristics of ILs make them potentially excellent candidates for battery electrolyte applications. IL-LiX electrolytes have a relatively high ionic conductivity. The very low to negligible vapor pressure of ILs at ambient pressure permits the use of polymeric pouches for batteries rather than the metal cans now used which saves on both manufacturing cost and battery weight. ILs can be easily dried under vacuum at elevated temperature, while conventional electrolyte solvents must be distilled and/or dried over molecular sieves, and then stored under rigorously controlled conditions to avoid moisture (water is unstable at the high voltages of Li-ion batteries).[45] But the strongest motivation for utilizing ILs in battery electrolytes stems from the combination of their exceptional electrochemical stability and low volatility/flammability.

Research on materials for Li-ion batteries has undergone explosive growth in the last decade. Current challenges for advanced battery development revolve around finding alternative electrode materials such as Sn- or Si-based alloy anodes and new metal oxide cathode materials, especially those suitable for high voltage applications (>4.3 V). The desire to increase the battery voltage (from the current 3.6 V with $LiCoO_2$) stems from the need to increase the battery energy density for plug-in hybrid electric vehicle (PHEV) applications. Greater energy density will reduce the size and cost for the batteries which is crucial for reducing the overall cost of the PHEV vehicles (the cost of the battery can be half or more of that of the total vehicle). Unfortunately, the current state-of-the-art electrolytes, which work well for small commercial Li-ion batteries, are unsuitable for these new high-voltage electrode materials. Further, the safety concerns mentioned above associated with the state-

of-the-art electrolytes largely preclude their use in the very large batteries required for PHEVs where thermal management is much more problematic. Alternative electrolyte materials must therefore be found for PHEV Li-ion batteries, yet the range of materials suitable for such high-voltage electrolytes is quite limited. Compounding this search is the need to also improve battery safety by reducing or eliminating the use of volatile/flammable organic solvents. Thus, a tremendous amount of attention has been focused in recent years on IL-based electrolytes.

References

1. Linden, D.; Reddy, T. B., Eds. *Handbook of Batteries*, 3rd edition, McGraw-Hill: New York, 2001.
2. Vincent, C. A.; Scrosati, B., Eds. *Modern Batteries: An Introduction to Electrochemical Power Sources*, 2nd edition, John Wiley & Sons, Inc.: New York, 1997.
3 Jasinski, R. *High Energy Batteries*, Plenum Press: New York, 1967.
4. Fraioly, A. V.; Barber, W. A.; Feldman, A. M. U.S. Patent 3,551,205, 1970.
5. Schneider, A. A.; Moser, J. U.S. Patent 3,674,562, 1972.
6. Moser, J. U.S. Patent 3,660,163, 1972.
7. Fukuda, M.; Ijima, T. *Power Sources, Vol. 5*; Collins, D. H., Ed.; Academic Press: London, 1975.
8. Koch, V. R.; Young, J. H. *J. Electrochem. Soc.* **1978**, *125*, 1371.
9. Yoshimatsu, I.; Hirai, T.; Yamaki, J. *J. Electrochem. Soc.* **1988**, *135*, 2422.
10. Xu, K. *Chem. Rev.* **2004**, *104*, 4303.

11. Broadhead, J.; Trumbore, F. A. *Power Sources, Vol. 5*; Collins, D. H., Ed.; Academic Press: London, 1975.

12. Aurbach, D.; Gofer, Y.; Langsam, J. *J. Electrochem. Soc.* **1989**, *136*, 3198.

13. Dominey, L. A. *Nonaqueous Electrochemistry*; Aurbach, D., Ed.; Marcel-Dekker: New York, 1999.

14. Armand, M. *Materials for Advanced Batteries*; Murphy, D. W., Broadhead, J., Steele, B. C. H., Eds.; Plenum Press: New York, 1980.

15. Ohzhku, T.; Ueda, A.; Nagayama, M. *J. Electrochem. Soc.* **1993**, *140*, 1862.

16. Bittihn, R.; Herr, R.; Hoge, D. *J. Power Sources* **1993**, *43/44*, 223.

17. Nagaura, T.; Nagamine, M.; Tanabe, I.; Miyamoto, N. *Prog. Batteries Sol. Cells* **1989**, *8*, 84.

18. Nagaura, T.; Ozawa, K. *Prog. Batteries Sol. Cells* **1990**, *9*, 209.

19. Nishi, Y.; Azuma, H.; Omaru, A. U.S. Patent 4,959,281, 1990.

20. Nagaura, T. *Proceedings of the 5th International Seminar on Lithium Battery Technology and Applications*, Deerfield Beach, FL, March 5-7, 1990; Florida Educational Seminars, Inc.: Boca Raton, FL.

21. Dahn, J. R.; von Sacken, U.; Fong, R. *Extended Abstracts of the 178th Electrochemical Society Meeting*, Seattle, WA, Oct. 1419, 1990; Abstract No. 42; Electrochemical Society: Pennington, NJ.

22. Broussely, M. *11th International Meeting on Lithium Batteries,* Monterey, CA, June 23-28, 2002; Abstract No. 415; Electrochemical Society: Pennington, NJ.

23. Scrosati, B. *Nat. Nanotechnol.* **2007**, *2*, 598.

24. Balakrishnan, P. G.; Ramesh, R.; Kumar T. P. *J. Power Sources* **2006**, *155*, 401.

25. von Sacken, U.; Nodwell, E.; Sundher, A.; Dahn, J. R. *Solid State Ionics* **1994**, *69*, 284.

26. Levy, S. C.; Bro, P. *Battery Hazards and Accident Prevention*, Plenum Press: New York, 1994.

27. Tobishima, S.; Yamaki, J. I. *J. Power Sources* **1999**, *882*, 81.

28. Arora, P.; Zhang, Z. *Chem. Rev.* **2004**, *104*, 4419.

29. Yang, H.; Zhuang, G. V.; Ross Jr., P. N. *J. Power Sources* **2006**, *161*, 573.

30. Wang, Q.; Sun, J.; Yao, X.; Chen, C. *Thermochim. Acta* **2005**, *437*, 12.

31. Hammami, A.; Raymond, N.; Armand, M. *Nature* **2003**, *424*, 635.

32. Foropoulos, J.; DesMarteau, D. *Inorg. Chem.* **1984**, *23*, 3720.

33. Dominey, L. A.; Koch, V. R.; Blakley, T. J. *Electrochim. Acta* **1992**, *37*, 1551.

34. Yang, H.; Kwon, K.; Devine T.; Evans, J. W. *J. Electrochem. Soc.* **2000**, *147*, 4399.

35. Krause, L. J.; Lamanna, W.; Summerfield, J.; Engle, M.; Korba, G.; Loch, R.; Atanasoski, R. *J. Power Sources* **1997**, *68*, 320.

36. Kanamura, K.; Umegaki, T.; Shiraishi, S.; Ohashi, M.; Takehara, Z. *J. Electrochem. Soc.* **2002**, *149*, A185.

37. Wasserscheid, P.; Welton, T., Eds. *Ionic Liquids in Synthesis*, 2nd edition, Wiley-VCH Verlag GmbH & Co. kGaA: Weinheim, 2008.

38. Welton, T. *Chem. Rev.* **1999**, *99*, 2071.

39. Huddleston, J. G.; Visser, A. E.; Reichert, W. M.; Willauer, H. D.; Broker, G. A.; Rogers, R. D. *Green Chem.* **2001**, *3*, 156.

40. Chiappe, C.; Pieraccini, D. *J. Phys. Org. Chem.* **2005**, *18*, 275.

41. Greaves, T. L.; Weerawardena, A.; Fong, C.; Krodkiewska, I.; Drummond, C. J. *J. Phys. Chem. B.* **2006**, *110*, 22479.

42. Nuthakki, B.; Greaves, T. L.; Krodkiewska, I.; Weerawardena, A.; Burgar, M, I.; Mulder, R. J.; Drummond, C. J. *Aust. J. Chem.* **2007**, *60*, 21.

43. Paulechka, Y. U.; Zaitsau, D. H.; Kabo, G, J.; Strechan, A. A. *Thermochim. Acta* **2005**, *439*, 158.

44. Morris, R. E. *Angew. Chem. Int. Ed.* **2008**, *47*, 442.

45. van Schalkwijk, W.; Scrosati, B., Eds. *Advances in Lithium-Ion Batteries*, Kluwer Academic/Plenum Publishers: New York, 2002.

Chapter 2. Experimental Procedures

2.1 Materials

1-Methylpyrrolidine ($C_5H_{11}N$, 97%), 1-methylimidazole ($C_4H_6N_2$, 99%) and various alkyliodides were purchased from Aldrich and used as-received. LiTFSI was purchased from 3M Company (St. Paul, MN) and lithium bis(fluorosulfonyl)imide (LiFSI) was purchased from Dai-ichi Kogyo, Seiyaku Co., Ltd (Japan). The salts were dried at 120°C under vacuum for 12 hrs. before use.

2.2 Sample Preparation

The experimental procedure utilized for the synthesis of all of the ILs was similar to that used for the *N*-methyl-*N*-alkylpyrrolidinium bis(trifluoromethanesulfonyl)imide ($PY_{1R}TFSI$) salts: 1-methylpyrrolidine was combined with a stoichiometric amount of alkyliodide (i.e., 1-iodopropane for $PY_{13}TFSI$) in ethyl acetate to synthesize the $PY_{1R}I$ precursors (Fig. 2-1). These reactions are highly exothermic and can be very fast for shorter alkyl chain lengths.[1] Thus, ethyl acetate is used as a solvent to both absorb the heat produced during the reaction and dilute the solution, thereby slowing the reaction rate. An ice bath was also sometimes used during this step to further slow the reaction to prevent or reduce side-reactions resulting in the formation of contaminants. Care was taken to minimize exposure of

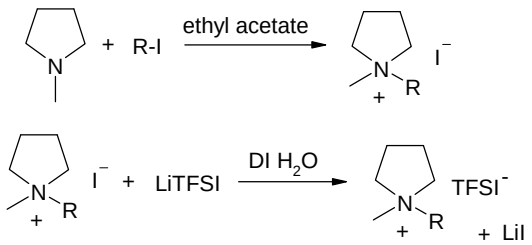

Fig. 2-1. Synthesis procedure for the $PY_{1R}TFSI$ ILs.

the reagents to light and oxygen due to the reactivity of the alkyliodides. The resulting white or yellow crystalline $PY_{1R}I$ salts were washed to remove unreacted reagents and contaminants with fresh ethyl acetate 5 times (using a separation funnel) until pure white salts were obtained.

The second step of the IL synthesis involved a metathesis reaction in which the I^- anion was exchanged with the $TFSI^-$ anion. The iodide salts and LiTFSI are soluble in water, but the ILs are not. Thus, if these salts are mixed in water, the ILs will separate from the solution as a new liquid phase leaving LiI in the aqueous phase (Fig. 2-1). Therefore, the purified $PY_{1R}I$ salts were dissolved in deionized (DI) water resulting in clear, colorless solutions. Stoichiometric amounts of LiTFSI dissolved in DI water were added and the mixtures were stirred to ensure complete mixing. The resulting aqueous phase with dissolved LiI was then removed and the remaining ILs were washed 8 times with fresh DI water to purity the $PY_{1R}TFSI$ salts. The salts were then heated while stirring on a hot plate for several hours at 120-140°C to remove most of the residual water. To remove other impurities, activated carbon was added and the mixtures were stirred on a hot plate at 140°C for 48 hours. The mixtures were then cooled to room temperature, ethyl acetate was added to dilute the solutions and they were then filtered through an activated alumina column to remove the activated carbon (and impurities). The ethyl acetate was then removed by a rotary evaporator. Finally, the ILs were under vacuum dried at 120°C overnight and the temperature was then increased to 140°C for another 8 hours (to remove the residual ethyl acetate and water). After purification and drying, the $PY_{1R}TFSI$ (R = 3-5) salts are clear, colorless liquids at room temperature. The materials were stored in hermetically sealed bottles in a N_2 glovebox.

IL-LiX mixtures were prepared in the glove box by combining the appropriate amounts of the $IM_{10R}TFSI$ or $PY_{1R}X$ and LiX salts (X = $TFSI^-$ or FSI^-) in a vial, and then heated on a hot plate while stirring to form homogeneous mixtures. The resulting IL-LiX mixtures were generally clear, colorless and odorless with moisture content below 10 ppm (tested by Karl-Fischer titration). The materials were stored in hermetically-sealed glass vials in the glovebox.

2.3 Instruments and Techniques

^{1}H NMR spectra were used to identify the structure of the ILs and verify their purity (Figs. 2-2, 2-3 and Table 2-1). All NMR spectra were measured at room temperature on a Varian Gemini 200 MHz Spectrometer. Deuterated acetonitrile (CD_3CN, 99.8 atom% D, containing 1% v/v TMS) was used as the solvent to dissolve the samples (the ILs are insoluble in $CDCl_3$). The ^{1}H NMR spectrum of pure

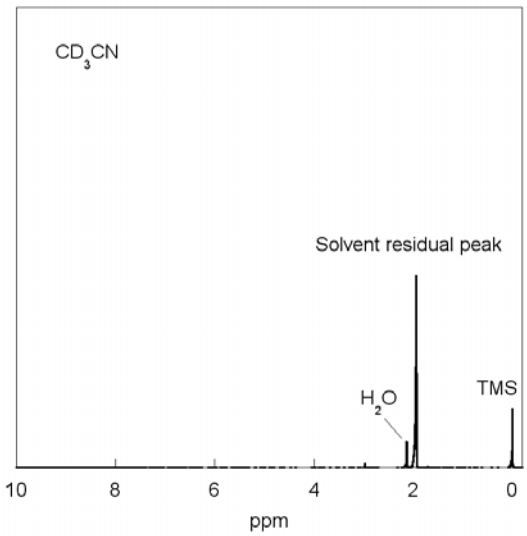

Fig. 2-2. ^{1}H NMR spectrum for CD_3CN.

Table 2-1. ^{1}H NMR data for $IM_{10R}TFSI$ (R = 1, 2, and 4) and $PY_{1R}TFSI$ (R = 3-5), δ_H (200 MHz, CD_3CN).

$IM_{101}TFSI$	8.37 (s, 1H), 7.32 (d, 2H), 3.82 (s, 6H)
$IM_{102}TFSI$	8.40 (s, 1H), 7.38 (s, 1H), 7.32 (s, 1H), 4.16 (q, 2H), 3.81 (s, 3H), 1.45 (t, 3H)
$IM_{104}TFSI$	8.42 (s, 1H), 7.38 (t, 1H), 7.34 (t, 1H), 4.13 (t, 2H), 3.83 (s, 3H), 1.79 (qnt, 2H), 1.32 (sext, 2H), 0.94 (t, 3H)
$PY_{13}TFSI$	3.42 (s, 2H, N-CH_2-ring), 3.40 (s, 2H, N-CH_2-ring), 3.18 (qnt, 2H, N-CH_2), 2.94 (s, 3H, N-CH_3), 2.15 (s, 2H, CH_2-ring), 2.14 (s, 2H, CH_2-ring), 1.76 (sept, 2H, CH_2), 0.96 (t, 3H, CH_3)
$PY_{14}TFSI$	3.40 (m, 4H, N-CH_2-ring), 3.22 (qnt, 2H, N-CH_2), 2.94 (s, 3H, N-CH_3), 2.16 (m, 4H, CH_2-ring), 1.72 (sept, 2H, CH_2), 1.36 (sext, 2H, CH_2), 0.96 (t, 3H, CH_3)
$PY_{15}TFSI$	3.40 (m, 4H, N-CH_2-ring), 3.22 (qnt, 2H, N-CH_2), 2.94 (s, 3H, N-CH_3), 2.15 (m, 4H, CH_2-ring), 1.73 (qnt, 2H, CH_2), 1.34 (m, 4H, CH_2), 0.92 (t, 3H, CH_3)

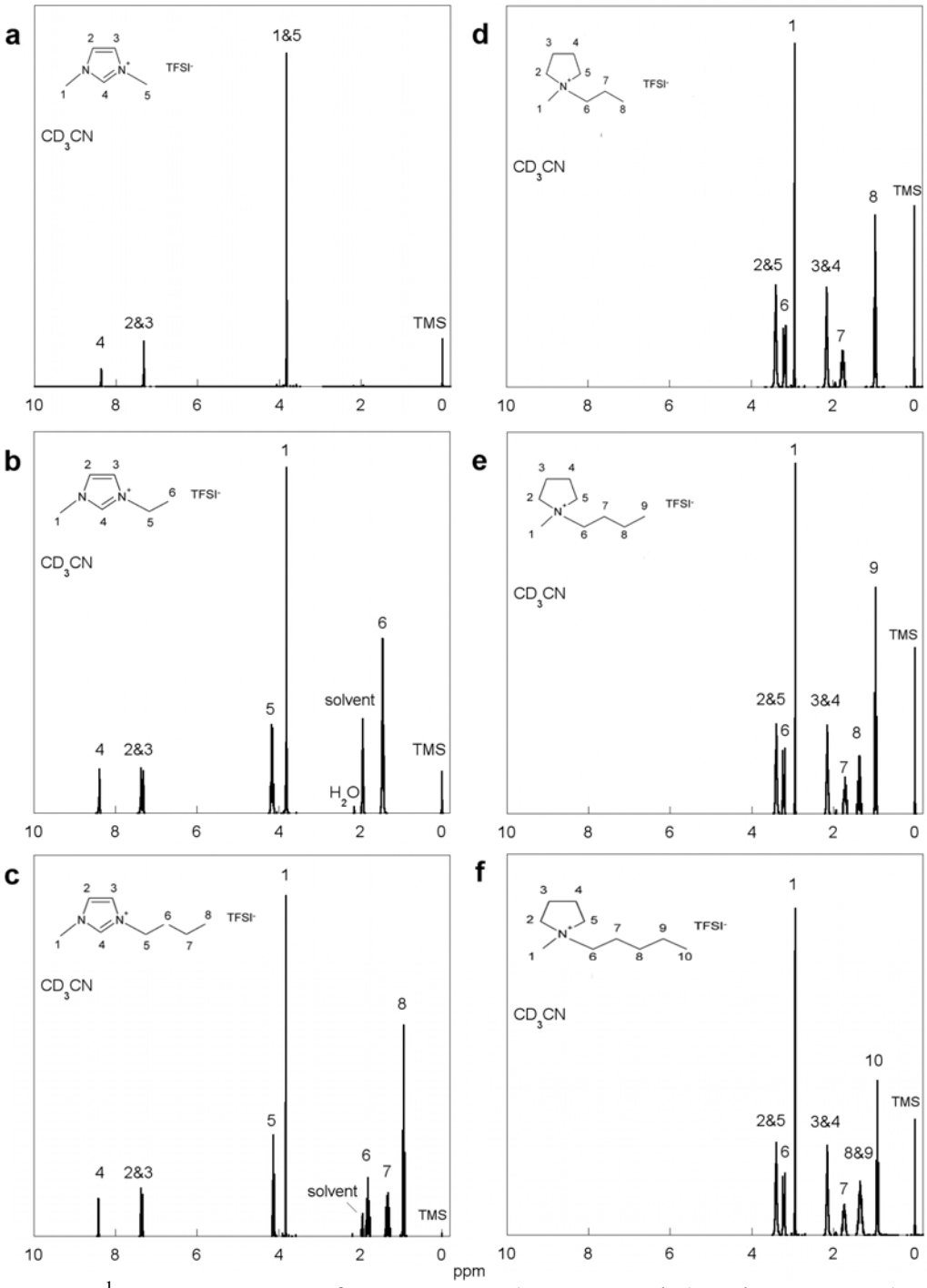

Fig. 2-3. ^{1}H NMR spectrum for $IM_{10R}TFSI$ (R = 1, 2 and 4) and $PY_{1R}TFSI$ (R = 3-5), δ_H (200 MHz, CD_3CN).

CD_3CN has a peak at 1.94 ppm due to impurities such as CHD_2CN, while a small amount of

water is detected at 2.13 ppm (Fig. 2-2).[2] ^{1}H NMR spectra for the $IM_{10R}TFSI$ and $PY_{1R}TFSI$ (Figs. 2-3 and Table 2-1) salts indicate that the ILs are of electrochemical grade purity. The water concentration of the ILs was determined using a Mettler Toledo Karl Fischer Coulometer DL39. The ILs were stored in the glove box prior to Karl Fischer analysis and then transferred into the instrument quickly. The water concentration of all of the samples was below 20 ppm.

DSC measurements were performed using either a TA Instruments Q1000 or Q2000 differential scanning calorimeter with liquid N_2 cooling. The instruments were calibrated with cyclohexane (solid-solid phase transition at -87.06°C, melt transition at 6.54°C) and indium (melt transition at 156.60°C). Hermetically sealed Al pans were prepared in the glove box. Typically, samples pans were slowly cooled (5°C min^{-1}) to -150°C and then heated (5°C min^{-1}) to 100°C or higher temperature (determined by the composition of the sample). It was sometimes necessary to cycle the samples in the DSC at various subambient temperatures in order to fully crystallized the samples. Some of the sample pans were also stored in a freezer prior to analysis and then transferred into the instrument quickly (to aid in crystallization for slowly nucleating samples).

TGA measurements were performed using a TA Instruments Q5000 thermogravimetric analyzer. The thermal stability was initially analyzed by heating from room temperature to 600°C (variable-temperature measurements) under either an air or N_2 atmosphere (>99.99%, water concentration 2-5 ppmv). Selected samples were then analyzed isothermally at different temperatures for 900 min. under an N_2 atmosphere to determine the long term stability of the materials at a given temperature.

Viscosity measurements were conducted using a SVM 3000 Stabinger viscometer. The tests were performed from 15-100°C with a 1°C min^{-1} heating rate. Measurements were taken in 5°C steps. At least 2.6 ml sample sizes were needed for the measurements and great care was taken to not expose the samples to air (and thus water) prior to and during the measurements. Ethyl acetate and N_2 gas (>99.99%, water concentration 2-5 ppmv) were used to clean the instrument after the measurements and the water concentration of the samples was tested before and after the measurements.

References

1. Appetecchi, G. B.; Scaccia, S.; Tizzani, C.; Alessandrini, F.; Passerini, S. *J. Electrochem. Soc.* **2006**, *153*, A1685.
2. Earle, M. J.; Esperança, J. M. S. S.; Gilea, M. A.; Canongia Lopes, J. N.; Rebelo, L. P. N.; Magee, J. W.; Seddon, K. R.; Widegren, J. A. *Nature* **2006**, *439*, 831 (see Supplementary Data).

Chapter 3. Ionic Liquids

3.1 Introduction

There is only a limited amount of data available in the literature regarding the physical properties of IL-based electrolytes.[1] The thermal properties and phase behavior of the neat ILs containing 1-alkyl-3-methylimidazolium (IM_{10R}^+, R = 1, 2 and 4) or *N*-alkyl-*N*-methylpyrrolidinium (PY_{1R}^+, R = 3-5) cations with the $TFSI^-$ anion (Fig. 3-1) are therefore examined in this chapter. The imidazolium cations, such as IM_{102}^+, are known to have a relatively low electrochemical stability (both cathodically and anodically).[2-4] In contrast, ILs with pyrrolidinium cations, such as PY_{13}^+ or PY_{14}^+, and $TFSI^-$ have been demonstrated as effective electrolyte materials for Li metal and Li-ion batteries.[5-10] Both classes of ILs are examined here to explore how the variation in the cation structure influences the properties (as IM_{10R}TFSI ILs are known to have a higher ionic conductivity than PY_{1R}TFSI ILs). The focus on ILs with this anion is due to the fact that a wide variety of cations form low melting salts with $TFSI^-$ (i.e., the T_m of the $PY_{14}X$ salts are PY_{14}TFSI: -18°C or -7°C (see below), $PY_{14}PF_6$: 70°C and $PY_{14}BF_4$: 150°C).[11-13] In Chapter 1, it was noted that LiTFSI in aprotic solvents has been found to corrode Al current collectors. There is, however, preliminary evidence which suggests that Al corrosion in IL-LiTFSI mixtures is inhibited.[14-16]

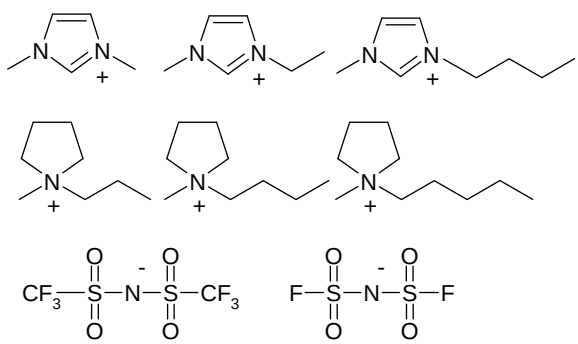

Fig. 3-1. Chemical structures of IM_{10R}^+ (R = 1, 2 and 4) and PY_{1R}^+ (R = 3-5) cations and $TFSI^-$ and FSI^- anions.

Recently, a new set of ILs based upon the bis(fluorosulfonyl)imide ($N(SO_2F)_2^-$ or FSI^-) anion has attracted strong interest.[6,7,17,18] A variety of synthesis techniques have been reported for the FSI^- anion[19-29] and the crystal structures are known for LiFSI, KFSI and CsFSI.[20,30,31] $IM_{102}FSI$ is reported to have a low T_m of -13°C, a viscosity of 18-25 cP and a high conductivity of 15.4-16.5 mS cm^{-1} (at 25°C) (a very low viscosity and high conductivity, respectively, for ILs).[6,7] At present, however, only a few reports are available regarding the physical characteristics of $PY_{1R}FSI$ ILs. Therefore, the physical and thermal properties of the $PY_{13}FSI$ and $PY_{14}FSI$ ILs (Fig. 3-1) are reported here in addition to the information regarding the $TFSI^-$ salts.

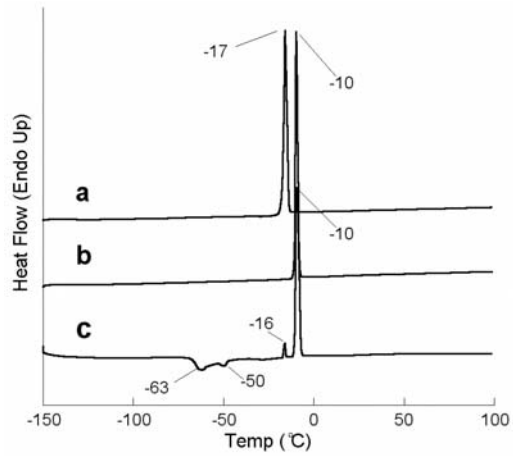

Fig. 3-2. DSC heating traces (5°C min^{-1}) of $IM_{102}TFSI$: (a)-(c) are for different thermal histories (see text).

3.2 $IM_{10R}TFSI$ (R = 1, 2 and 4) ILs

The $IM_{102}TFSI$ salt has polymorphic thermal phase behavior with at least two different crystalline phases able to form depending upon the thermal history of the salt. This is demonstrated in Fig. 3-2 using three different DSC experiments to crystallize $IM_{102}TFSI$: initially (Fig. 3-2a), the sample was cooled slowly (5°C min^{-1}) from room temperature to -150°C, and then heated to 100°C, with the T_m found at -17°C. The sample was then (Fig. 3-2b) quickly cooled (20°C min^{-1}) to -150°C, heated and annealed at -30°C for 5 min., cooled to -150°C and heated to 100°C. This procedure instead resulted in a single peak for the T_m at -10°C. The same sample was then rapidly quenched to -150°C (resulting in partial crystallization) and heated to 100°C (Fig. 3-

2c). In this case, the partially amorphous sample began to crystallize near -65°C. Two melting peaks at -16 and -10°C were then noted. This can be explained by the formation of two different crystalline phases for $IM_{102}TFSI$ - one is a thermodynamically favorable $IM_{102}TFSI$ (IA) phase formed during slow cooling with a T_m at -16°C, while the second is a kinetically favorable $IM_{102}TFSI$ (IB) phase with a T_m at -10°C.[32] The crystal structures for both crystalline phases are known. In each structure, the IM_{102}^+ cations have the same conformation, but the $TFSI^-$ anions have different conformations with either C_1 or C_2 symmetry (Fig. 3-3) resulting in considerable different packing of the ions in the crystals.[33-37] In contrast to $IM_{102}TFSI$, the $IM_{101}TFSI$ and $IM_{104}TFSI$ salts have relatively simple phase behavior. No solid-solid phase transitions were found when heating $IM_{101}TFSI$ and $IM_{104}TFSI$ from -150°C to 100°C, and only a single T_m is noted at 24°C and 3°C, respectively, for the two salts.

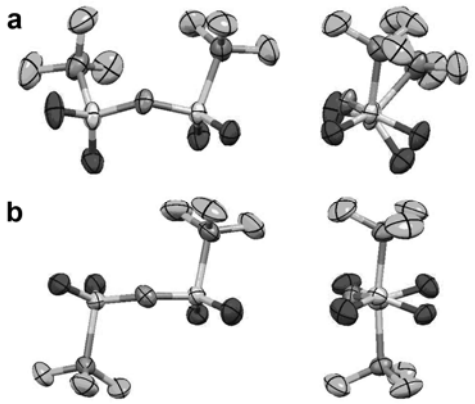

Fig. 3-3. $TFSI^-$ anion conformations. (a) C_1 conformer and (b) C_2 conformer (two views of each shown).

The thermal stability of the $IM_{10R}TFSI$ salts was analyzed using both variable-temperature and isothermal TGA measurements. Fig. 3-4 indicates that the onset point for mass loss (1wt%) is about 308-310°C for $IM_{101}TFSI$, 272-275°C

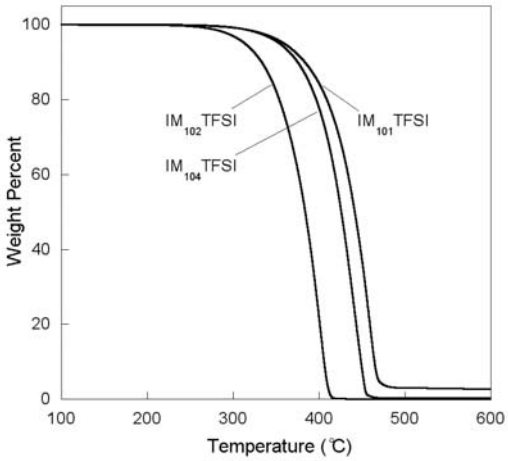

Fig. 3-4. Variable-temperature TGA traces (5°C min^{-1}) of $IM_{10R}TFSI$ (N_2 atmosphere).

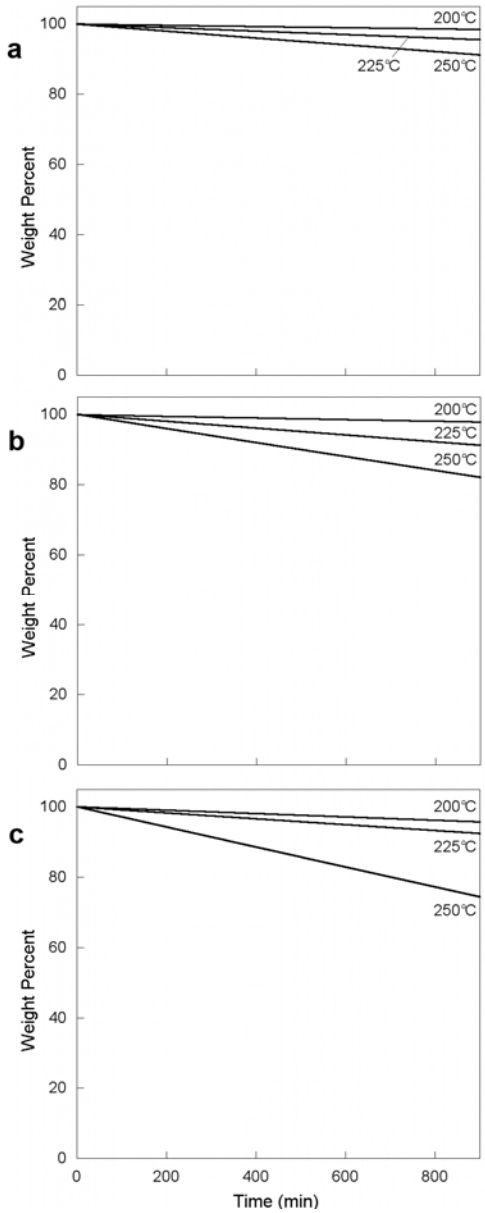

Fig. 3-5. Isothermal TGA traces of (a) $IM_{101}TFSI$, (b) $IM_{102}TFSI$ and (c) $IM_{104}TFSI$ (N_2 atmosphere). The temperature for each measurement is indicated in the figure.

for $IM_{102}TFSI$ and 308-310°C for $IM_{104}TFSI$. There is no mass remaining after decomposition when the salts were heated to 600°C under an N_2 atmosphere for the $IM_{102}TFSI$ and $IM_{104}TFSI$ salts. For the $IM_{101}TFSI$ salt, however, approximately 3 wt% of the original mass remains after decomposition when heated under an N_2 atmosphere. The isothermal TGA measurements (900 min.) indicate that ILs loose approximately 5-8 wt% of their mass on heating at 200 or 225°C. Heating to a higher temperature results in a greater mass loss. The straight lines for the mass loss in Fig. 3-5 suggests that there is no nucleation process occurring leading to rapid decomposition (see below for the FSI^- ILs).

The viscosity of ILs is mainly governed by the electrostatic attraction between the cations and anions, the tendency to form hydrogen

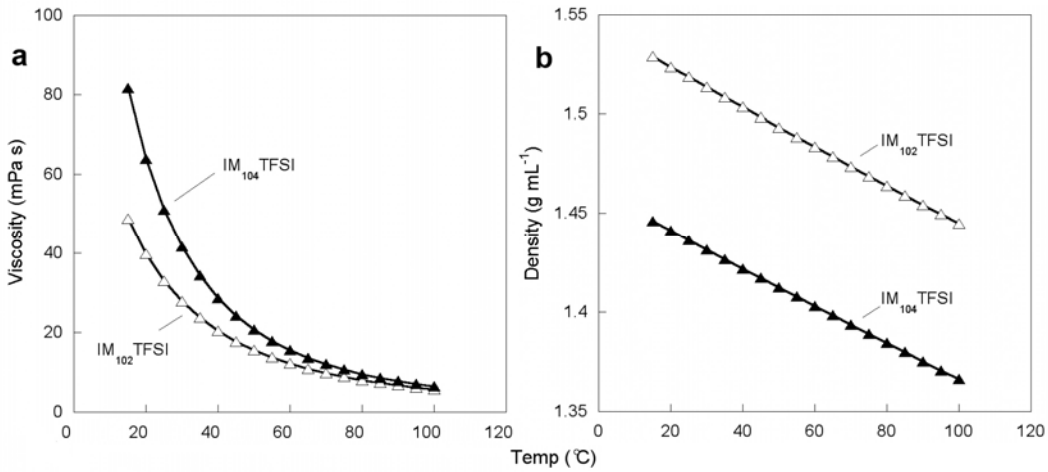

Fig. 3-6. Variable-temperature (a) viscosity and (b) density of $IM_{10R}TFSI$ (R = 2,4).

bonds, the strength of Van der Waals interactions and the degrees of freedom within the ions.[38-50] Fig. 3-6a compares the variable-temperature viscosity of the $IM_{10R}TFSI$ ILs. The following equations fit the data between 15-100°C:

$$IM_{102}TFSI: \eta = 86.585 - (3.3154)T + (5.9173e^{-2})T^2 - (5.1148e^{-4})T^3 + (1.7064e^{-6})T^4$$

$$IM_{104}TFSI: \eta = 157.85 - (6.8127)T + (1.292\ e^{-1})T^2 - (1.1535e^{-3})T^3 + (2.9186e^{-6})T^4$$

where the units are η (mPa·s) and T (°C). There is a significant difference in the viscosity of the two ILs at lower temperature with the $IM_{102}TFSI$ IL much less viscous than $IM_{104}TFSI$. Heating both ILs to higher temperature, however, results in a nearly identical viscosity at 100°C. The viscosity of ILs has generally been found to increase with increasing alkyl side chain length possibly due to the increase of Van der Waals interactions.[51]

Fig. 3-6b shows the density of both ILs as a function of temperature over the range 15-100°C. The density of both ILs linearly decreases with increasing temperature and increased with decreasing alkyl side chain length, as expected.

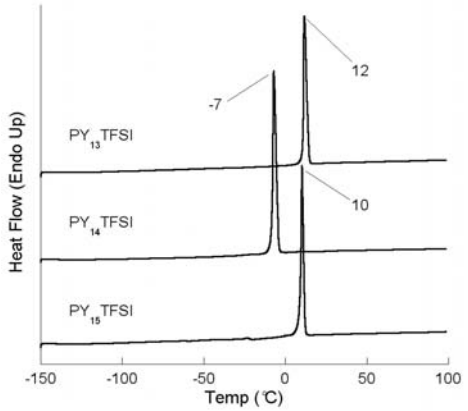

Fig. 3-7. DSC heating traces (5°C min^{-1}) of $PY_{1R}TFSI$ (R = 3-5).

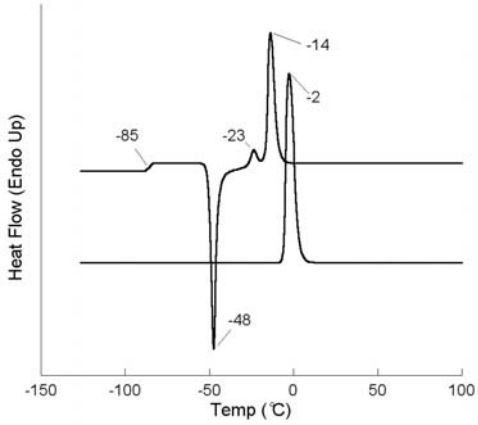

Fig. 3-8. DSC heating traces (10°C min^{-1}) of $PY_{14}TFSI$ after quenching (top) or slow cooling/annealing (bottom) from room temperature.[1]

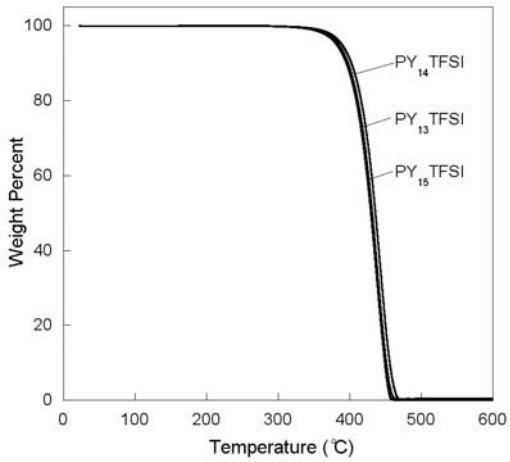

Fig. 3-9. Variable-temperature TGA traces (5°C min^{-1}) of $PY_{1R}TFSI$ (N_2 atmosphere).

3.3 $PY_{1R}TFSI$ (R = 3-5) ILs

The $PY_{1R}TFSI$ (R = 3-5) salts are room temperature ILs which melt at 12, -7 and 10°C (Fig. 3-7), respectively. $PY_{13}TFSI$ was reported to have a solid-solid phase transition.[52] However, this interesting phenomenon was not found in our laboratory. A metastable phase may account for the differences in the previously reported and observed phase behavior of this salt.[1] $PY_{14}TFSI$ was reported to have a solid-solid phase transition at -24°C followed by a T_m at -18°C.[53] In contrast, only a single melting peak at -7°C was found in our laboratory. Henderson *et al.* noted that if the salt is supercooled and cold-crystallized relatively rapidly during the heating scan, a thermal behavior similar to that previously reported is found (Fig. 3-8).[1] This suggests that a metastable $PY_{14}TFSI$ crystalline phase forms as noted for $IM_{102}TFSI$ above. $PY_{15}TFSI$, however, does not appear to be

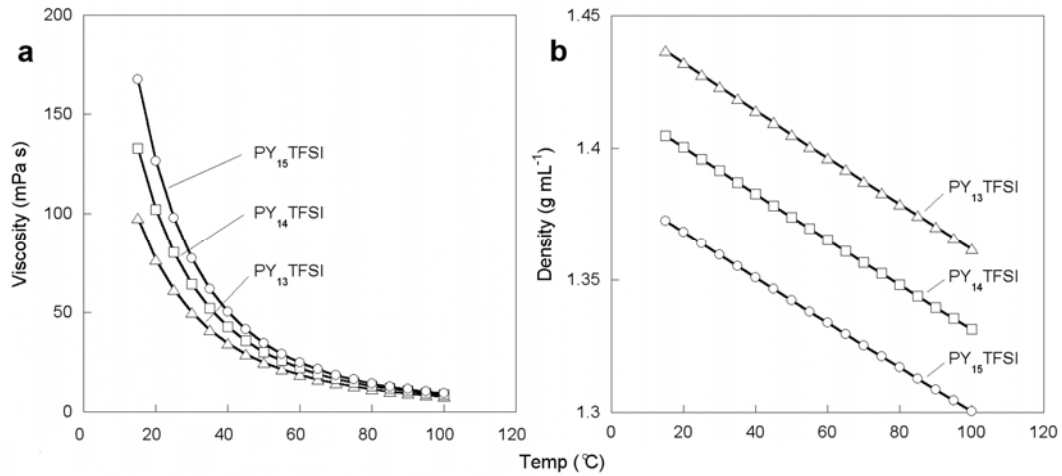

Fig. 3-10. Variable-temperature (a) viscosity and (b) density of $PY_{1R}TFSI$ (R = 3-5).

polymorphic as there is no indication of a second crystalline phase occurring for this salt.

Fig. 3-9 indicates that the onset point for mass loss (1 wt%) is approximately 350°C for the $PY_{1R}TFSI$ (R = 3-5) salts, which demonstrates that these ILs are significantly more thermally stable than the $IM_{10R}TFSI$ ILs. No mass remained for these salts after decomposition when heated to 600°C under an N_2 atmosphere.

Fig. 3-10a compares the variable-temperature viscosity of the $PY_{1R}TFSI$ ILs. The following equations fit the data between 15-100°C:

$$PY_{13}TFSI: \eta = 189.16 - (8.1506)T + (1.5439e^{-1})T^2 - (1.3774e^{-3})T^3 + (4.6772e^{-6})T^4$$

$$PY_{14}TFSI: \eta = 266.43 - (12.018)T + (2.3275e^{-1})T^2 - (2.1007e^{-3})T^3 + (7.1781e^{-6})T^4$$

$$PY_{15}TFSI: \eta = 345.76 - (16.147)T + (3.1841e^{-1})T^2 - (2.9028e^{-3})T^3 + (9.9803e^{-6})T^4$$

where the units are η (mPa·s) and T (°C). The longer alkyl chain results in a larger viscosity as noted for the $IM_{10R}TFSI$ ILs. At high temperature, however, the viscosity of the ILs with different chain lengths, as for the $IM_{10R}TFSI$ salts, becomes nearly the same. The $PY_{1R}TFSI$ salts are more viscous than the $IM_{10R}TFSI$ salts.

Fig. 3-10b shows the density of the ILs as a function of temperature over the range 15-100°C. As for the $IM_{10R}TFSI$ salts, the density decreases linearly with increasing temperature and increases with decreasing alkyl side chain length.

3.4 $PY_{1R}FSI$ (R = 3 and 4) ILs

The $PY_{13}FSI$ and $PY_{14}FSI$ ILs have a low T_m, low viscosity, high conductivity and relatively high electrochemical stability making them desirable materials for many electrochemical technologies.[54] Unfortunately, as shown here, these salts have a lower thermal stability than the corresponding $TFSI^-$ based ILs, but the stability is still acceptable for most applications. The following work was published in:

Zhou, Q.; Henderson, W. A.; Appetecchi, G. B.; Montanino, M.; Passerini, S. *J. Phys. Chem. B* **2008,** *112,* 13577.

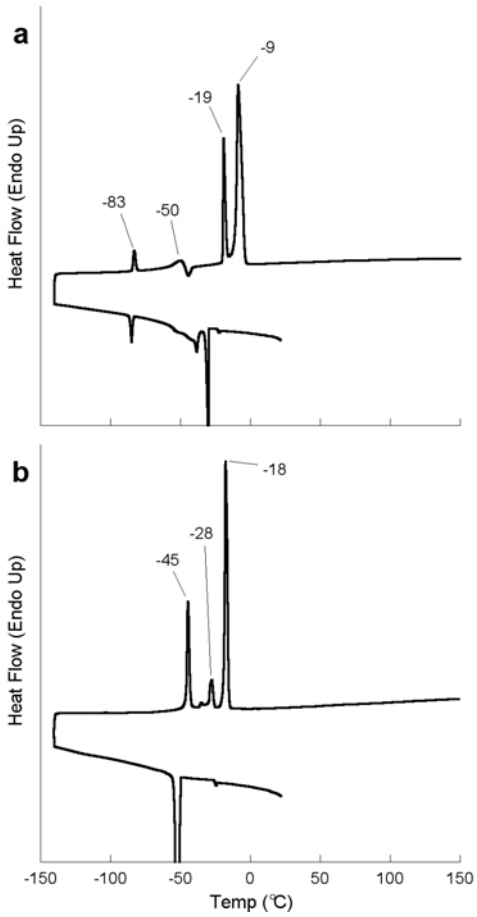

Fig. 3-11. DSC cooling and heating traces (5°C min^{-1}) of (a) $PY_{13}FSI$ and (b) $PY_{14}FSI$.

DSC heating and cooling traces for $PY_{13}FSI$ and $PY_{14}FSI$ are shown in Fig. 3-11. Although both salts significantly supercool (hysteresis between the T_m and crystallization temperature), crystallization does occur readily on cooling. In

fact, it was not possible to quench the salts into an amorphous phase using cooling rates up to 40°C min^{-1}. In all cases the salts crystallized. $PY_{13}FSI$ undergoes several exothermic transitions on cooling (Fig. 3-11a). On heating, multiple endothermic transitions were observed including a low energy solid-solid phase transition (phase III-II) with a peak at -83°C, a solid-solid phase transition at -19°C (phase II-I) and a T_m at -9°C (phase I-L). The identity of the broad endothermic transition with a peak temperature of -50°C and subsequent exothermic transition near -45°C is not clear. These latter transitions were reproducible in some scans and completely absent (flat baseline) in others. One possibility is that the peak at -50°C corresponds to the crystallization of another (kinetic) phase which is dependent upon the thermal history of the salt. After melting this phase (at -50°C), the resulting liquid then crystallizes (the exothermic transition) into the thermodynamically-stable phase II structure. Thermal decomposition occurs on heating the $PY_{13}FSI$ IL above 150°C. The T_m of $PY_{13}FSI$ has been previously reported to be -18°C.[6] The method used to determine this T_m was not provided. It is possible that the onset of the solid-solid phase transition was mistakenly identified as the onset of melting.

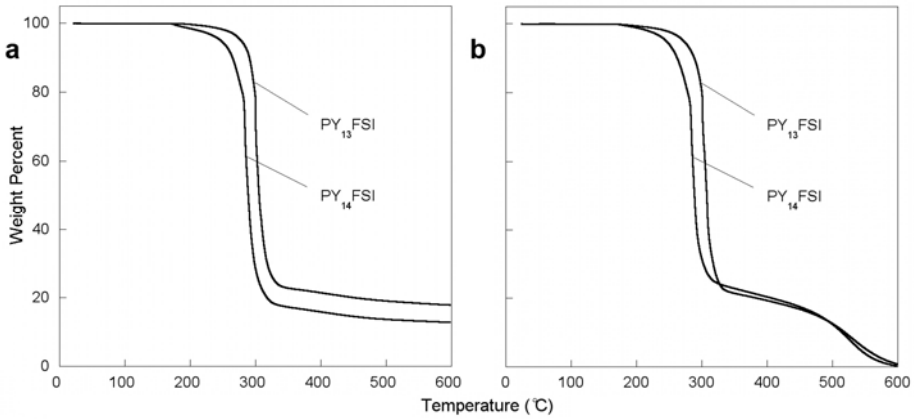

Fig. 3-12. Variable-temperature TGA traces (5°C min^{-1}) of $PY_{1R}FSI$: (a) N_2 and (b) air atmosphere.

$PY_{14}FSI$ also undergoes several endothermic transitions on heating (Fig. 3-11b). Sharp endothermic transitions at -45, -28 and -18°C correspond to a phase III-II, phase II-I and phase I-L (T_m) transitions, respectively. The identity of the small peak near -34°C is not clear. This peak is not found to be reproducible in repeated heating/cooling traces. It may be that this peak is associated with a kinetically (but not thermodynamically) stable phase as suggested above for $PY_{13}FSI$. The thermal stability of the ILs was analyzed using both variable-temperature and isothermal TGA measurements. Fig. 3-12 indicates that the initial mass loss for both ILs is independent of the atmosphere (air or N_2). The onset point for mass loss (1 wt%) is about 219-231°C for $PY_{13}FSI$ and 189-198°C for $PY_{14}FSI$. Approximately 15-20 wt% of the original IL remains after decomposition when heated under an N_2 atmosphere. If, instead, air is present, a second thermal process beginning near 400°C and finishing near 600°C which leads to the complete volatilization of the thermal degradation products (Fig. 3-12b). The isothermal TGA measurements indicate that neither IL looses mass on storage at 100°C for 24 hrs (Fig. 3-13). Both ILs, however, loose approximately 9-10 wt% of their mass on

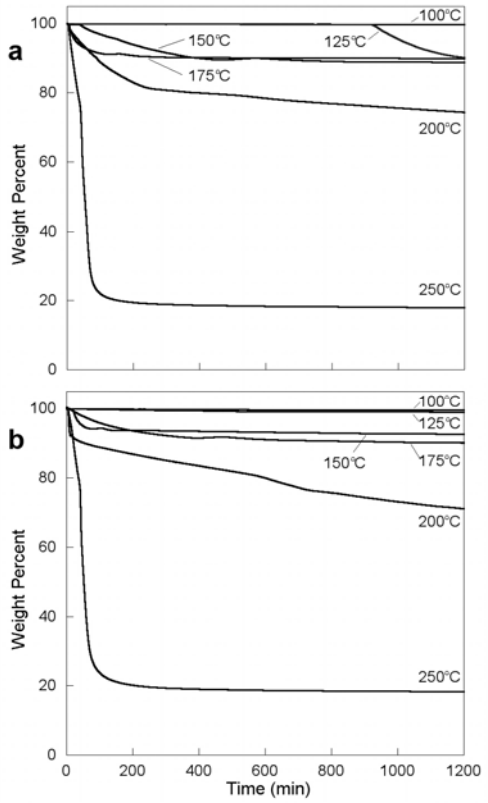

Fig. 3-13. Isothermal TGA traces of $PY_{1R}FSI$: (a) R = 3 and (b) R = 4 (N_2 atmosphere). The temperature for each measurement is indicated in the figure.

heating at 150 or 175°C. Note that $PY_{14}FSI$ did not loose any significant mass on heating at 125°C, whereas $PY_{13}FSI$ did, but only after a long delay. This suggests that a nucleation process occurs for the decomposition. The data further suggest that the same degradation mechanism occurs for both ILs up to 175°C resulting in a thermally stable degradation product. Heating to higher temperature, however, leads to greater mass loss. Heating both ILs at 250°C results in an initial rapid mass loss down to about 18 wt% after which the mass loss is minor in agreement with the variable temperature data (for an N_2 atmosphere). Note that the thermal degradation behavior of the FSI^- salts (Fig. 3-13) differs markedly from that of the $TFSI^-$ salts (Fig. 3-5 - data for the $PY_{1R}TFSI$ salts not shown, but is similar to the $IM_{10R}TFSI$ salts with increased stability) for which the thermal degradation was linear with time at a given temperature.

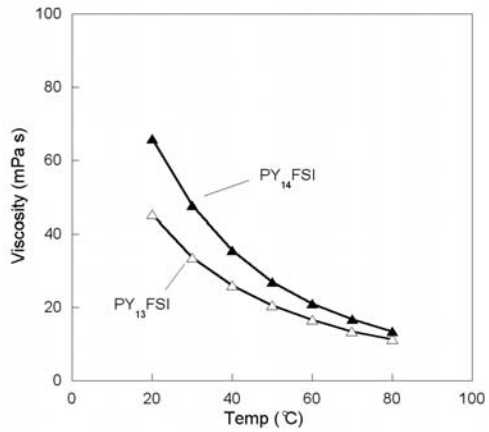

Fig. 3-14. Variable-temperature viscosity of $PY_{1R}FSI$ (R = 3,4).

Fig. 3-14 compares the variable-temperature viscosity of the ILs. These measurements were performed by a collaborator in Italy using a rheometer.[50] The following equations fit the data between 20-80°C:

$$PY_{13}FSI: \eta = 89.561 - (3.1808)T + (5.9269e^{-2})T^2 - (5.7737e^{-4})T^3 + (2.2585e^{-6})T^4$$

$$PY_{14}FSI: \eta = 129.39 - (4.3875)T + (7.1815e^{-2})T^2 - (6.0301e^{-4})T^3 + (2.0577e^{-6})T^4$$

where the units are η (mPa·s) and T (°C). The higher viscosity of $PY_{14}FSI$, relative to $PY_{13}FSI$, may account for the lower conductivity of the former (see Chapter 4). The viscosity of $PY_{13}FSI$ is intermediate between the previously reported viscosity (mPa·s) values of 40

(25°C),[7] 53 (25°C)[6] and 39 (20°C).[17] Note that the $PY_{13}FSI$ and $PY_{14}FSI$ salts are much less viscous than the corresponding ILs with the $TFSI^-$ anion.

References

1. Henderson, W. A.; Passerini, S. *Chem. Mater* **2004**, *16***,** 2881.
2. Sakaebe, H.; Matsumoto, H.; Tatsumi, K. *J. Power Sources* **2005**, *146*, 693.
3. Matsumoto, H.; Sakaebe, H.; Tatsumi, K. *J. Power Sources* **2005**, *146*, 45.
4. Sakaebe, H.; Matsumoto, H.; Tatsumi, K. *Electrochim. Acta* **2007**, *53*, 1048.
5. Shin, J.-H.; Henderson, W. A.; Scaccia, S.; Prosini, P. P.; Passerini, S. *J. Power Sources* **2006**, *156*, 560.
6. Ishikawa, M.; Sugimoto, T.; Kikuta, M.; Ishiko, E.; Kono, M. *J. Power Sources* **2006**, *162*, 658.
7. Matsumoto, H.; Sakaebe, H.; Tatsumi, K.; Kikuta, M.; Ishiko, E.; Kono, M. *J. Power Sources* **2006**, *160*, 1308.
8. Shin, J.-H.; Henderson, W. A.; Passerini, S. *Electrochem. Solid-State Lett.* **2005**, *8*, A125.
9. Shin, J-H.; Henderson, W. A.; Tizzani, C.; Passerini, S.; Jeong, S-S.; Kim, K-W. *J. Electrochem. Soc.* **2006**, *153*, A1649.
10. Appetecchi, G. B.; Scaccia, S.; Tizzani, C.; Alessandrini, F.; Passerini, S. *J. Electrochem. Soc.* **2006**, *153*, A1685.
11. Zhou, Z.-B.; Matsumoto, H.; Tatsumi, K. *Chem. Eur. J.* **2006**, *12*, 2196.
12. Golding, J.; Hamid, N.; MacFarlane, D. R.; Forsyth, M.; Forsyth, C.; Collins, C.; Huang, J. *Chem. Mater*. **2001**, *13*, 558.

13.Foryth, S.; Golding, J.; MacFarlane, D. R.; Forsyth, M. *Electrochim. Acta* **2001**, *46*, 1753.

14. Garcia, B.; Armand, M. *J. Power Sources* **2004**, *132*, 206.

15. Peng, C.; Yang, L.; Zhang, Z.; Tachibana, K.; Yang, Y. *J. Power Sources* **2007**, *173*, 510.

16.Peng, C.; Yang, L.; Zhang, Z.; Tachibana, K.; Yang, Y.; Zhao, S. *Electrochim. Acta* **2008**, *53*, 4764.

17. Guerfi, A.; Duchesne, S.; Kobayashi, Y.; Vijh, A.; Zaghib, K. *J. Power Sources* **2008**, *175*, 866.

18. Saint, J.; Best, A. S.; Hollenkamp, A. F.; Kerr, J.; Shin, J.-H.; Doeff, M. M. *J. Electrochem. Soc*. **2008**, *155*, A172.

19. Beran, M.; Prihoda, J. Z. *Anorg. Allg. Chem*. **2005**, *631*, 55.

20. Beran, M.; Prihoda, J.; Zak, Z.; Cernik, M. *Polyhedron* **2006**, *25*, 1292.

21.Appel. R.; Becke-Goehring, M.; Eisenhauer, G.; Hartenstein, J. *Chem. Ber*. **1962**, *95*, 625.

22. Appel, R.; Ritterbader, H. *Chem. Ber*. **1964**, *97*, 849.

23. Lustig, M.; Bumgarder, C. L.; Johnson, F. A.; Ruff, J. K. *Inorg. Chem*. **1964**, *3*, 1165.

24. Ruff, J. *Inorg. Chem*. **1965**, *4*, 1446.

25. Ruff, J. K. *Inorg. Chem*. **1967**, *6*, 2108.

26. Roesky, H. W.; Hoff, A. *Chem. Ber*. **1968**, *101*, 162.

27. Glemser, O.; Roesky, H. W. Inorg. Nucl. *Chem. Lett*. **1968**, *4*, 179.

28. Ruzicka, A.; Kotasova, I. Z. *Chem*. **1987**, *27*, 180.

29. Vij, A.; Kirchmeier, R. L.; Shreeve J. M.; Verma, R. D. Coord. *Chem. Rev*. **1997**, *158*, 413.

30. Hiemisch, O.; Henschel, D.; Blaschette, A.; Jones, P. G. Z. *Anorg. Allg. Chem*. **1997**, *623*, 324.

31. Krumm, B.; Vij, A.; Kirchmeier, R. L.; Shreeve, J. M. *Inorg. Chem*. **1998**, *37*, 6295.

32. Henderson, W. A. *Unpublished work.*

33. Foropoulos Jr., J.; DesMarteau, D. D. *Inorg. Chem*. **1984**, *23*, 3720.

34. Arnaud, R.; Benrabah, D.; Sanchez, J.-Y. *J. Phys. Chem*. **1996**, *100*, 10882.

35. Johansson, P.; Gejji, S. P.; Tegenfeldt, J.; Lindgren, J. *Electrochim. Acta* **1998**, *43*, 1375.

36. Holbrey, J. D.; Reichert, W. M.; Rogers, R. D. *Dalton Trans*. **2004**, 2267.

37. Rey, I.; Johansson, P.; Lindgren, J.; Lassègues, J. C.; Servant, L. *J. Phys. Chem. A* **1998**, *102*, 3249.

38. Bonhote, P.; Dias, A. P.; Papageorgiou, N.; Kalyanasundaram, K.; Graetzel, M. *Inorg. Chem*. **1996**, *35*, 1168.

39. McEwen, A. B.; Ngo, H. L.; LeCompte, K.; Goldman, J. L. *J. Electrochem. Soc*. **1999**, *146*, 1687.

40. Huddleston, J. G.; Visser, A. E.; Reichert, W. M.; Willauer, H. D.; Broker, G. A.; Rogers, R. D. *Green Chem*. **2001**, *3*,156.

41. Branco, L. C.; Rosa, J. N.; Ramos, J. J. M.; Afonso, C. A. M. *Chem. Eur. J.* **2002**, *8*, 3671.

42. Dzyuba, S. V.; Bartsch, R. A. *ChemPhysChem* **2002**, *3*, 161.

43. Hagiwara, R.; Matsumoto, K.; Nakamori, Y.; Tsuda, T.; Ito, Y.; Matsumoto, H.; Momota, K. *J. Electrochem. Soc*. **2003**, *15*0, D195.

44. Matsumoto, H.; Kageyama, H.; Miyazaki, Y. *Chem. Commun*. **2002**, 1726.

45. Xu, W.; Cooper, E. I.; Angell, C. A. *J. Phys. Chem. B* **2003**, *107*, 6170.

46. Sun, J.; Forsyth, M.; MacFarlane, D. R. *J. Phys. Chem. B* **1998**, *102*, 8858.

47. MacFarlane, D. R.; Meakin, P.; Sun, J.; Amini, N.; Forsyth, M. *J. Phys. Chem. B* **1999**, *103*, 4164.

48. Zhou, Z.-B.; Matsumoto, H.; Tatsumi, K. *Chem. Eur. J.* **2004**, *10*, 6581.

49. Zhou, Z.-B.; Matsumoto, H.; Tatsumi, K. *Chem. Lett.* **2004**, *33*, 680.

50. Zhou, Z.-B.; Matsumoto, H.; Tatsumi, K. *Chem. Eur. J.* **2005**, *11*, 752.

51. Zhou, Z.-B.; Matsumoto, H.; Tatsumi, K. *ChemPhysChem* **2005**, *6*, 1324.

52. Hill, A. J.; Huang, J.; Efthimiadis, J.; Meakin, P.; Forsyth, M.; MacFarlane, D. R. *Solid State Ionics* **2002**, *154-155*, 119.

53. MacFarlane, D. R.; Meakin, P.; Amini, N.; Forsyth, M. *J. Phys.: Condens. Matter* **2001**, *13*, 8257.

54. Zhou, Q.; Henderson, W. A.; Appetecchi, G. B.; Montanino, M.; Passerini, S. *J. Phys. Chem. B* **2008**, *112*, 13577.

Chapter 4. Ionic Liquid-Lithium Salt Electrolytes

4.1 Introduction

Many demonstrations have now been made for the replacement of aprotic solvents by ILs for Li metal and Li-ion battery electrolytes. For example, Holzapfel *et al.* reported reversible Li^+ cation intercalation into a graphite electrode using an $IM_{102}TFSI$-1M $LiPF_6$ electrolyte (containing 5 wt% of vinylene carbonate (VC) as a solvent additive).[1,2] The VC additive was necessary as it has been found that without it the organic cations (i.e., IM_{102}^+) intercalate into the graphite before the Li^+ cations do (at a higher potential). Most of these intercalated organic cations are then not deintercalated when the potential is reversed (e.g., the reaction is irreversible). To prevent this with $TFSI^-$-based ILs, an additive such as VC may be used which decomposes prior to the cation intercalation to create an SEI layer on the graphite which then prevents the organic cations from reaching the electrode, but still permits the transport of Li^+ cations. Thus, the use of additives enables such ILs to be used as replacements for solvents in electrolytes for Li-ion batteries.

As noted in the above example, a lithium salt (LiX) must be added to the IL for electroactive Li^+ cations to be present in the electrolyte for the battery reactions. At present, however, little is known about the thermal phase behavior and stability of IL-LiX electrolytes.[3] This has therefore been examined here for (1-x) $IM_{10R}TFSI$-(x) LiTFSI (R = 1, 2 and 4) mixtures for comparison with the previously reported phase behavior of (1-x) $PY_{1R}TFSI$-(x) LiTFSI (R = 2-4).[3]

The $IM_{102}FSI$ IL has been reported to have outstanding physicochemical properties, particularly for a battery electrolyte, with a high ionic conductivity, low viscosity and a low T_m.[4] LiTFSI was used as the LiX salt and there was no irreversible cathodic current peak (indicating organic cation intercalation) on a graphite negative electrode during charging, even without the addition of additives. The explanation for the excellent performance was that some of the FSI^- anions degraded to form an SEI (something that does not happen with $TFSI^-$ ILs) with high Li^+ cation conductivity. Guerfi *et al.* have also recently reported excellent cycling properties for a $PY_{13}FSI$-LiFSI electrolyte toward graphite.[5] However, no work is currently available regarding the detailed phase behavior and thermal properties of $PY_{1R}FSI$-LiFSI electrolytes. This is therefore reported here for a comparison with the $IM_{10R}TFSI$ and $PY_{1R}TFSI$ mixtures with LiTFSI.

4.2 (1-x) $IM_{10R}TFSI$-(x) LiTFSI Mixtures

DSC data for the preparation of the phase diagram for (1-x) $IM_{101}TFSI$-(x) LiTFSI are shown in Fig. 4-1a. Adding LiTFSI initially lowers the T_m of the mixture from that of the neat $IM_{101}TFSI$ salt. The data indicates that new mixed salts crystalline phases exist for x = 0.50 compositions (corresponding to 1/1 $IM_{101}TFSI$/LiTFSI complexes). The structures of these phases are not known, but the 1/1 phase may bear a resemblance to the 1/1 crystalline phases which have been reported for $IM_{102}CF_3SO_3/LiCF_3SO_3$ (Fig. 4-2) and $Et_3NHCF_3SO_3/LiCF_3SO_3$ mixtures.[6,7] In both of these structures, each anion is coordinated to two Li^+ cations. Each Li^+ cation, in turn, is coordinated by four oxygens - one each from four different anions. The result is polymeric $[Li^+...2(CF_3SO_3^-)]_n$ chains. For electrostatic

neutrality, surrounding these ion chains are the organic cations (either IM_{102}^+ or Et_3NH^+ cations) which have a single hydrogen bond to the third $CF_3SO_3^-$ anion oxygens (which are not coordinated to a Li^+ cation).

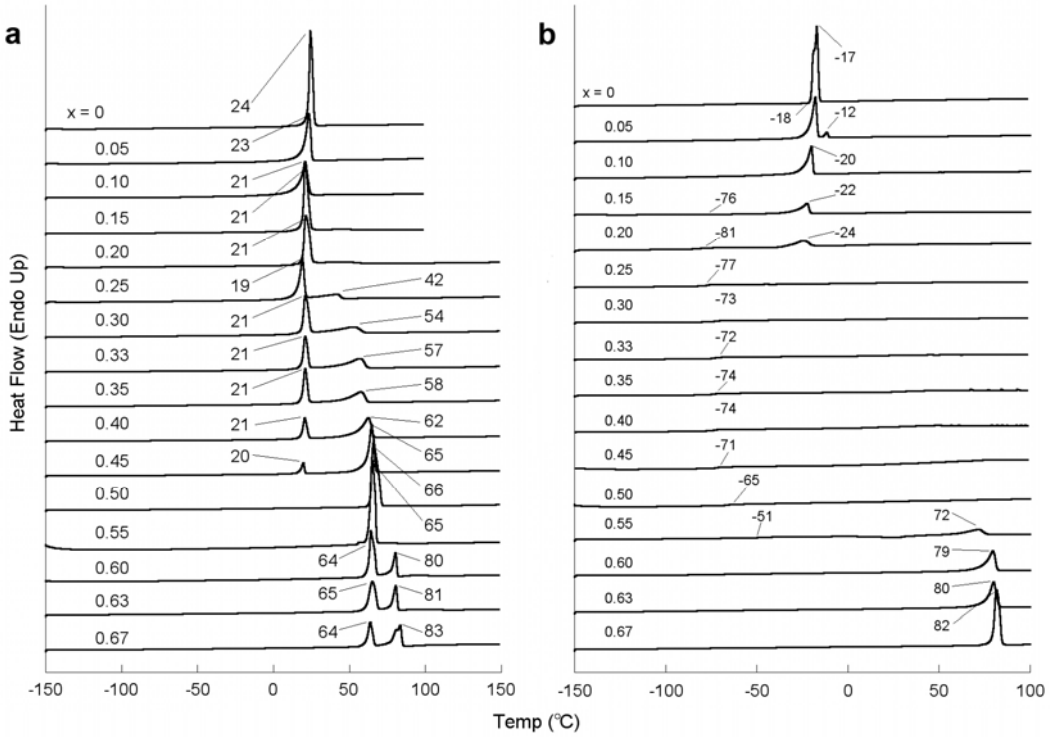

Fig. 4-1. DSC heat traces (5°C min^{-1}) of (1-x) $IM_{10R}TFSI$-(x) LiTFSI mixtures: (a) R = 1, (b) R = 2 and (c) R = 4 (peak and T_g temperatures are noted).

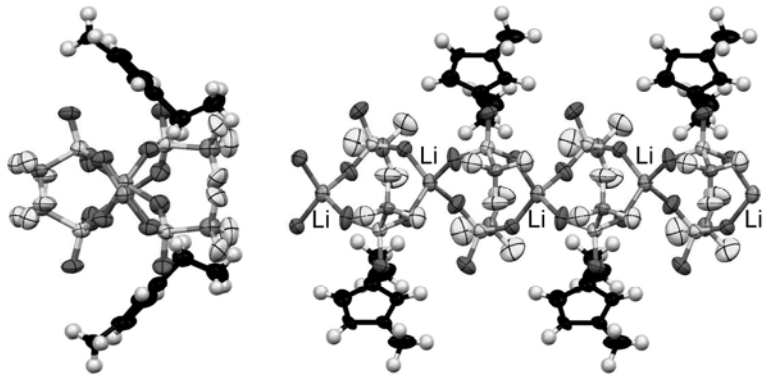

Fig. 4-2. Portion of the crystal structure of the (1-x) $IM_{102}CF_3SO_3$-(x) $LiCF_3SO_3$ (x = 0.50) (or 1/1 $IM_{101}CF_3SO_3/LiCF_3SO_3$) crystalline phase (two views shown).[6] The C and N atoms of the IM_{102}^+ cations are colored black for clarity.

The DSC data for (1-x) $IM_{102}TFSI$-(x) LiTFSI mixtures (Fig. 4-1b) indicate that as the LiTFSI mole fraction (x) increases, the crystallization process becomes more and more difficult, and no crystalline phase was observed for $0.25 \leq x \leq 0.50$. For the amorphous samples, the glass transition (T_g) tends to increase with increasing fraction of LiTFSI, as expected. A crystalline peak for an x = 0.67 crystalline phase (1/2 $IM_{102}TFSI$/LiTFSI complex) is observed for samples with x > 0.50. The crystal structure of this phase has been previously reported and is shown in Fig. 4-3.[8] The ions forms two dimensional planar sheets (a portion of one of these is shown in the figure) stacked together with principally the anion fluorine atoms separating the sheets. The Li^+ cations are coordinated by five oxygen atoms (from either three or four different $TFSI^-$ anions). Different anions are coordinated differently, but each anion has either three or all four of the oxygens atoms coordinated to a Li^+ cation thereby creating the planar sheets. The sheets (composed of Li^+ cations and $TFSI^-$ anions) result in the formation of cavities in which reside two uncoordinated IM_{102}^+ cations (Fig. 4-3).

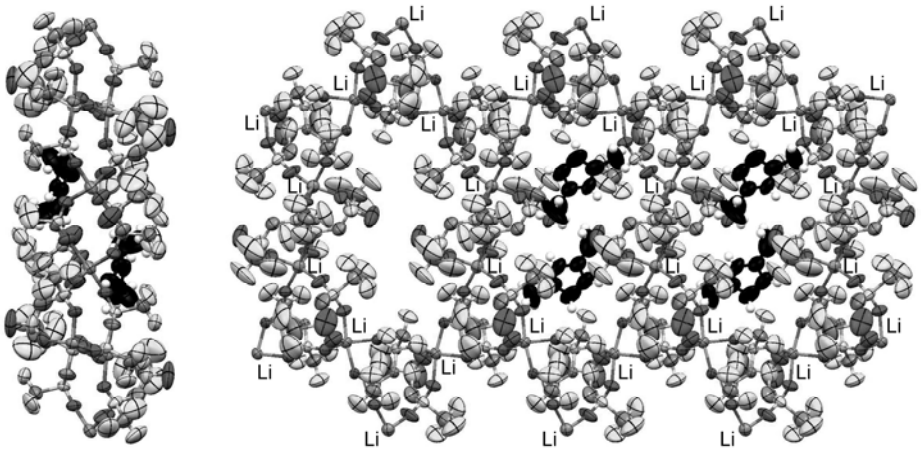

Fig. 4-3. Portion of the crystal structure of the (1-x) $IM_{102}TFSI$-(x) LiTFSI (x = 0.67) (or 1/2 $IM_{102}TFSI$/ LiTFSI) crystalline phase (two views). The C and N atoms of the IM_{102}^+ cations are colored black and the two cations have been removed from the left cavity for clarity.[8]

For the (1-x) $IM_{104}TFSI$-(x) LiTFSI mixtures, it was not possible to crystallize the samples when x > 0.15 using either slower cooling/heating rates (1°C min^{-1}) or by annealing the mixtures for extended periods of time at low temperature (Fig. 4-1c).

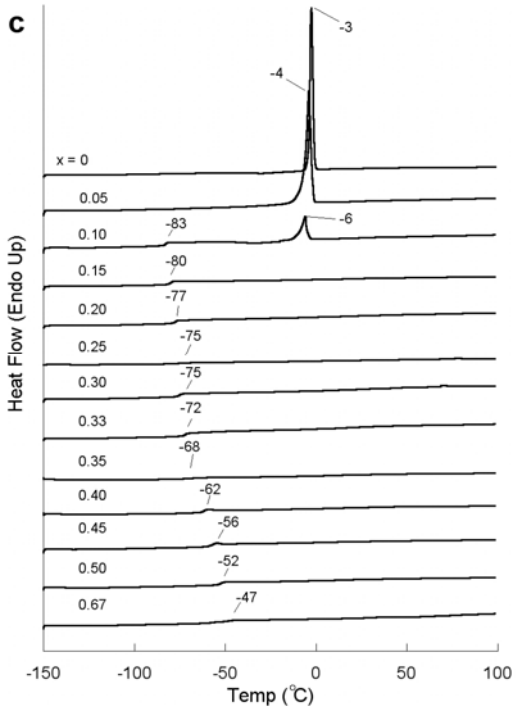

Fig. 4-1 (cont.).

Although many ILs are widely reported to have high thermal stability, there is actually only limited data available examining this property. We have performed both variable-temperature and isothermal TGA measurements to examine the thermal properties of the (1-x) $IM_{10R}TFSI$-(x) LiTFSI (R = 2 and 4) mixtures. The isothermal measurements provide a more accurate depiction of the actual resistance of the ILs to thermal degradation. The variable-temperature thermal stability measurements for (1-x) $IM_{10R}TFSI$-(x) LiTFSI mixtures are

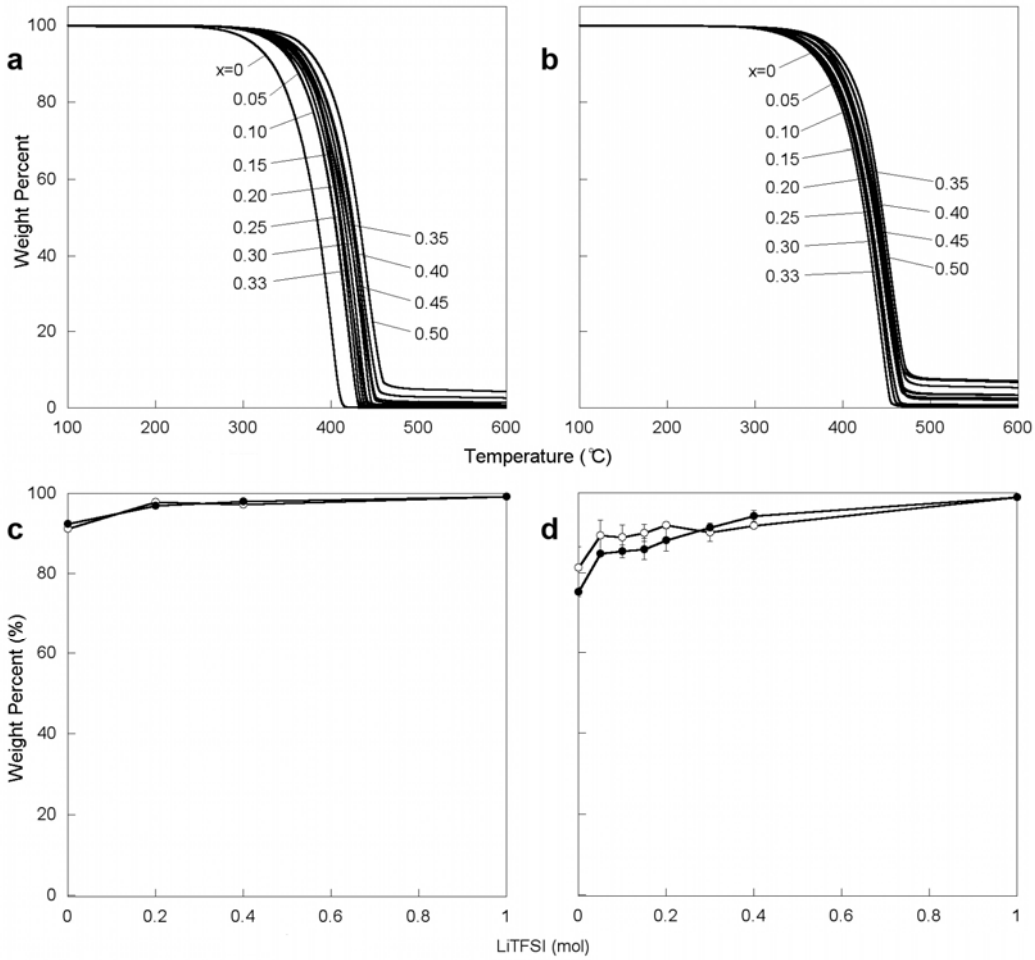

Fig. 4-4. Variable-temperature TGA traces (5°C min^{-1}) of (1-x) $IM_{10R}TFSI$-(x) LiTFSI mixtures (N_2 atmosphere): (a) R = 2 and (b) R = 4; and mass remaining for (1-x) $IM_{10R}TFSI$-(x) LiTFSI mixtures after isothermal TGA runs (N_2 atmosphere), open circles for R = 2 and filled circles for R = 4: (c) 225°C and (d) 250°C.

shown in Figs. 4-4a and 4b. The onset point for mass loss (1 wt%) is about 272-275°C for $IM_{102}TFSI$ and 308-310°C for $IM_{104}TFSI$ (Chapter 3). Interestingly, the onset temperature for mass loss of the mixtures is significantly increased with increasing LiTFSI concentration. For the x = 0.50 samples, the onset point for mass loss (1 wt%) is increased to 320°C and 331°C for $IM_{102}TFSI$ and $IM_{104}TFSI$, respectively, which is almost the same onset mass loss temperature as pure LiTFSI (Chapter 1). The isothermal TGA measurements of these mixtures are shown in Figs. 4-4c and 4d, indicating the relatively high thermal stability for these mixtures. The pure $IM_{10R}TFSI$ (R = 2 or 4) salts loose approximately 8-9 wt% of their mass on heating at 225°C. Adding LiTFSI increases their thermal stability noticeably with more than 95 wt% of their original mass of the mixtures remained after 900 min. Mixtures for both salts have comparable behavior on heating at 225°C. Heating to higher temperature, however, leads to greater mass loss. Heating mixtures at 250°C results in a mass loss of about 18 wt% and 25 wt%, respectively, for the pure $IM_{10R}TFSI$ (R = 2 or 4) salts. The addition of LiTFSI reduces this weight lost with a significant difference noted even for the addition of only 5 mol% LiTFSI (x = 0.05). The $IM_{102}TFSI$ mixtures are more thermally stable than the $IM_{104}TFSI$ mixtures for the $0 \leq x \leq 0.20$ samples. For the x = 0.30 and 0.40 samples, however, a larger mass loss occurs for $IM_{102}TFSI$ mixtures, but the difference is not large. Note that the error bars are relatively large (from repeated measurements) suggesting some variability is to be expected in such measurements.

The viscosity data (Fig. 4-5a) shows that adding LiTFSI induces an increase in the viscosity, especially for the $x \geq 0.40$ samples. There is a significant difference in the viscosity for both sets of mixtures below 80°C. Heating to higher temperature, however, results in only

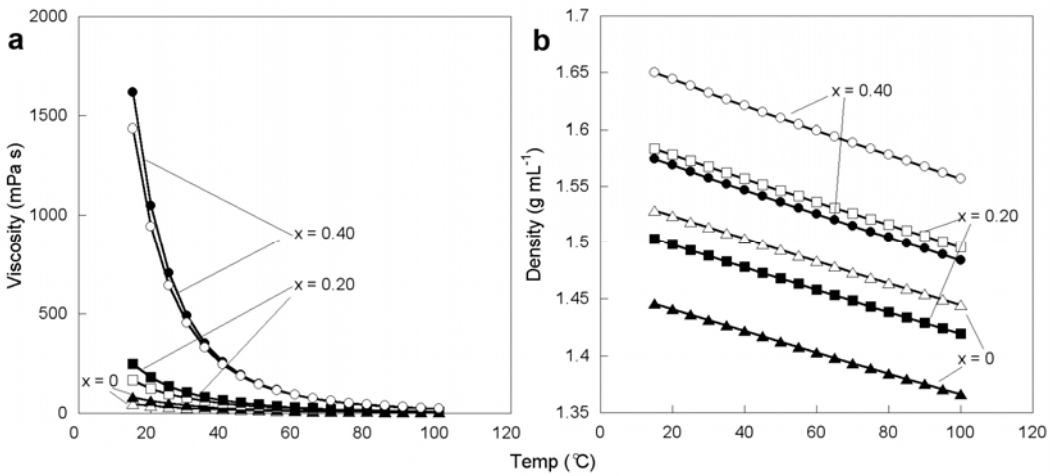

Fig. 4-5. Variable-temperature (a) viscosity and (b) density of (1-x) $IM_{10R}TFSI$-(x) LiTFSI mixtures (open symbols for R = 2 and filled symbols for R = 4).

a modest further reduction in the viscosity. Although differences are found in the viscosity of the two ILs with a given composition of LiTFSI at lower temperatures, these differences are negligible above about 40°C.

Fig. 4-5b shows the density of the samples as a function of temperature over the range 15-100°C. The addition of LiTFSI results in a substantial increase in the density with the $IM_{102}TFSI$ mixtures being denser than the $IM_{104}TFSI$ mixtures for a given concentration of LiTFSI.

4.3 (1-x) $PY_{1R}TFSI$-(x) LiTFSI Mixtures

The phase behavior of (1-x) $PY_{1R}TFSI$-(x) LiTFSI (R = 2-4) mixtures has been previously reported.[3] The DSC heating traces for these mixtures are shown in Fig. 4-6 for comparison with the data in Fig. 4-1 for the (1-x) $IM_{10R}TFSI$-(x) LiTFSI mixtures.

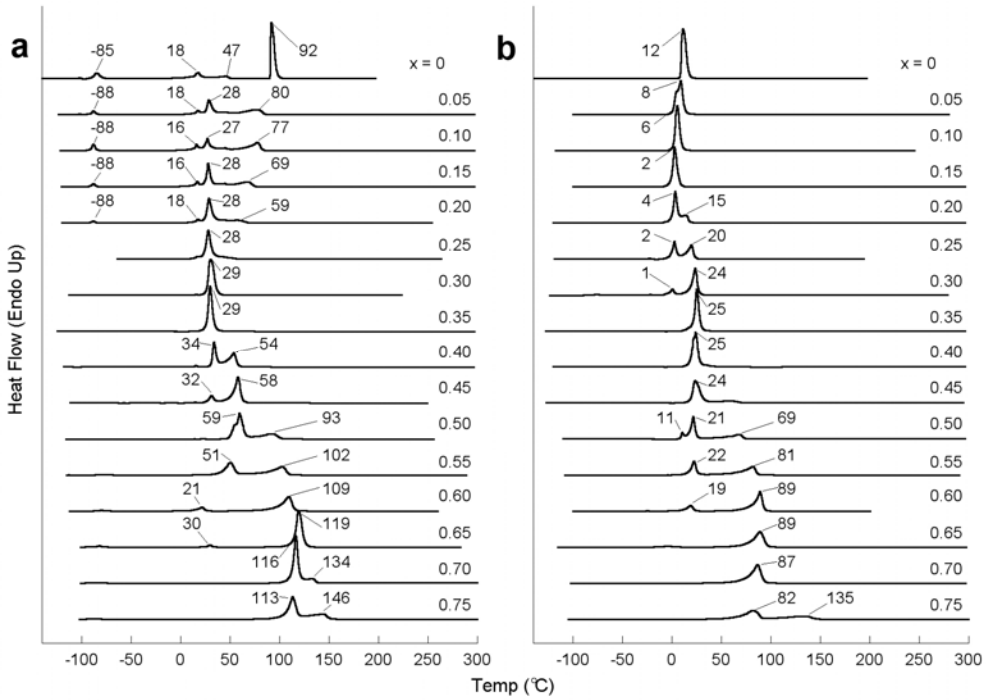

Fig. 4-6. DSC heating traces (5°C min^{-1}) of (1-x) $PY_{1R}TFSI$-(x) LiTFSI mixtures: (a) R = 2, (b) R = 3 and (c) R = 4 (peak and T_g temperatures are noted).[3]

The (1-x) $PY_{12}TFSI$-(x) LiTFSI mixture (Fig. 4-6a) has either a eutectic composition or a new crystalline (2/1 $PY_{12}TFSI$/LiTFSI) phase at a composition of x = 0.33 (this cannot be determined from the available thermal data). There is some evidence to suggest that a 1/1 (x = 0.50) phase also forms, although this may be metastable as it was not possible to form a homogeneous 1/1 phase for an x = 0.50 sample.[3] At higher LiTFSI concentration, an x

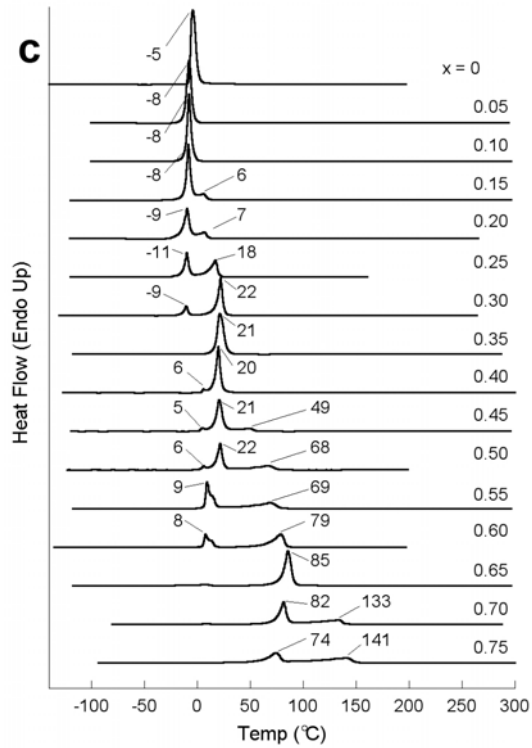

Fig. 4-6 (cont.).

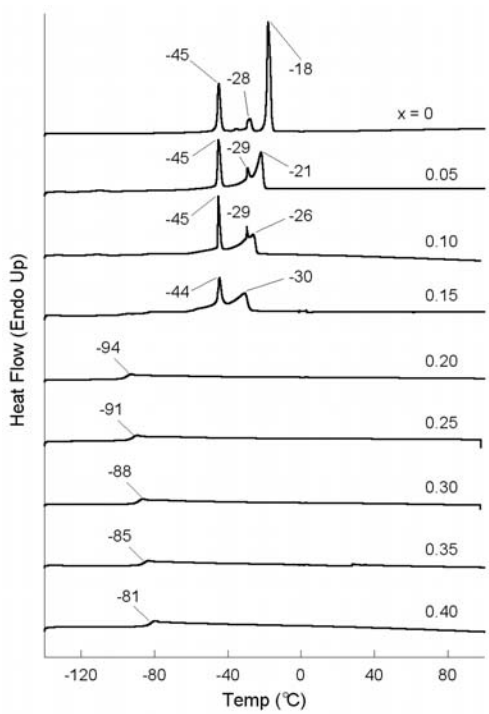

Fig. 4-7. DSC heating traces (5°C min^{-1}) of (1-x) $PY_{14}FSI$-(x) LiFSI (peak and T_g temperatures are noted).

= 0.67 (1/2 $PY_{12}TFSI$/LiTFSI) phase forms. For the $PY_{13}TFSI$ and $PY_{14}TFSI$ mixtures with LiTFSI (Figs. 4-6b and 6c), a 2/1 (x = 0.33) $PY_{1R}TFSI$/LiTFSI phase clearly forms as well as a 1/2 (x = 0.67) phase.

4.4 (1-x) $PY_{14}FSI$-(x) LiFSI Mixtures

Fig. 4-7 shows the DSC heating traces of (1-x) $PY_{14}FSI$-(x) LiFSI mixtures. The pure $PY_{14}FSI$ salt shows three endothermic peaks at -45, -28, and -18°C, corresponding to two solid-solid phase transitions and the melting of the $PY_{14}FSI$, respectively (Chapter 3).[9] The x = 0.05 and 0.10 samples show three similar peaks. The melting peak becomes broader and occurs at a lower temperature with increasing LiFSI concentration. The second solid-solid phase transition peak overlaps with the melting peak for the x = 0.15 sample. However, the first peak due to the solid-solid transition occurs at the same temperature. The crystallization process becomes more and more difficult with increasing LiFSI concentration, and no crystalline phase

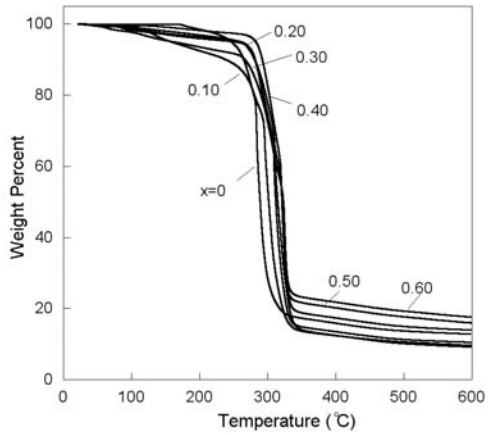

Fig. 4-8. Variable temperature TGA traces (5°C min^{-1}) of (1-x) $PY_{14}FSI$-(x) LiFSI mixtures (N_2 atmosphere).

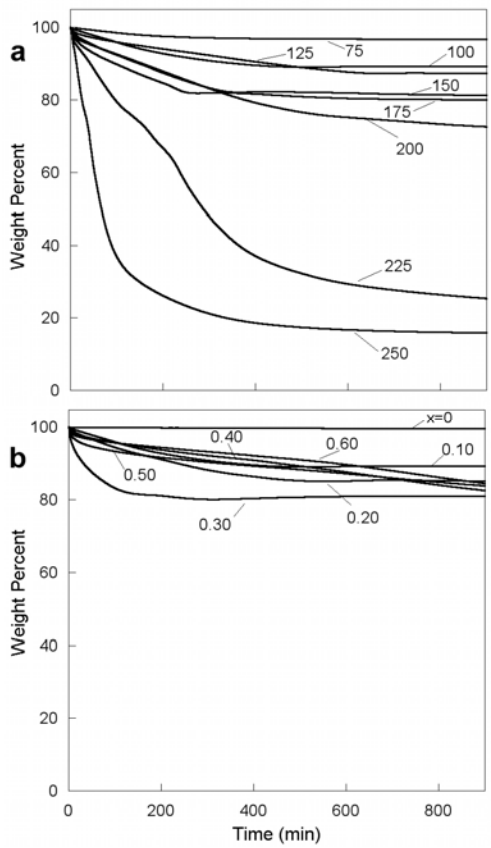

Fig. 4-9. Isothermal TGA traces for: (a) (1-x) $PY_{14}FSI$-(x) LiFSI (x = 0.10) (N_2 atmosphere). The temperature for each scan is indicated in the figure and (b) (1-x) $PY_{14}FSI$-(x) LiFSI mixtures at 100°C (N_2 atmosphere). Mole fraction is indicated in the figure.

was detected for x ≥ 0.20 samples, showing that, for the experimental procedures utilized, the electrolytes remained amorphous. Another interesting feature is the very low T_g measured for the amorphous samples (below -80°C), even for the x = 0.40 sample.

Fig. 4-8 shows that, in contrast with the ILs based upon the $TFSI^-$ anion, most of the samples have significant mass loss above 100°C. The long term thermal stability of these mixtures is shown in Fig. 4-9, indicating a relatively poor thermal stability for these mixtures, even at 75°C. Note that the pure $PY_{14}FSI$ salt was thermally stable up to 125°C for 24 hrs.[9] It is possible that impurities (if any) in the mixtures from the addition of the commercially available LiFSI salt result in this lower stability or instead the presence of the LiFSI may result in a rapid trace water contamination during loading of the samples from the glove box into the TGA instrument. There is no doubt, however, that the $-SO_2F$ group is far more reactive and thus less thermally stable than the $-SO_2CF_3$ group found in the $TFSI^-$ anion. Interestingly, although all of the samples containing LiFSI had a relatively lower thermal stability than that of the

pure $PY_{14}FSI$ salt, the onset of mass loss does not scale linearly with increasing LiFSI concentration.

The viscosity data (Fig. 4-10) show that the addition of LiFSI induces an increase in viscosity, especially for temperatures below 50°C, as for the IL-LiX mixtures based upon the $TFSI^-$ anion. The viscosity of the (1-x) $PY_{14}FSI$-(x) LiFSI mixtures is lower than the (1-x) $IM_{10R}TFSI$-(x) LiTFSI mixtures (Fig. 4-5a) and much lower than similar mixtures with $PY_{1R}TFSI$ salts (data not shown) for a given concentration of LiX salt.

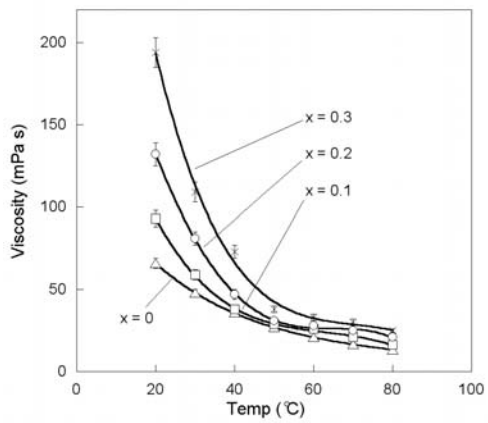

Fig. 4-10. Variable-temperature viscosity of (1-x) $PY_{14}FSI$-(x) LiFSI mixtures.

4.5 Discussion

A comparison of the phase behavior of the $IM_{10R}TFSI$ and $PY_{1R}TFSI$ salts with LiTFSI shows both similarities and differences in behavior. For example, there is no evidence that the $IM_{10R}TFSI$ salts form the 2/1 phase that is a predominant feature of the $PY_{1R}TFSI$ mixtures. The reason for this is unknown at present. There are no structural models (crystal structures) known for such a composition at present to aid in clarifying this. The $IM_{102}TFSI$ salt does, however, form the 1/2 phase which is also a common feature of the $PY_{1R}TFSI$ mixtures. The known structure for this phase indicates that cavities form in the Li^+...$TFSI^-$ anion planar lattice that hold two organic cations which remain uncoordinated. It is easy to envision that the cation can be readily replaced with another cation of similar size to create

the same phase with a different salt. Interestingly, the $IM_{104}TFSI$ salt does not form this phase. One explanation is that the IM_{104}^{+} cations are too large to fit within the cavities, but this does not explain why the $IM_{101}TFSI$ salt also does not form this phase (unless it is because the IM_{101}^{+} cations are too small and leave too much void space in the structure). The 1/1 phase forms readily for the $IM_{101}TFSI$ salt, but the $IM_{102}TFSI$ and $IM_{104}TFSI$ salts remain amorphous instead of forming a 1/1 phase. Once again, this may be an ion size/shape effect which prevents the ions from packing together in the optimal manner to form the 'preferred' structures. The amorphous phase may then be viewed as a 'frustrated' phase in which many of the ions have the same or similar coordination as found in the crystalline phases of similar composition, but the entire ensemble of the coordinated lattice cannot come together. There is no satisfactory explanation at present, however, for why the $PY_{14}FSI$-LiFSI mixtures do not form a crystalline phase (besides the crystallization of some of the $PY_{14}FSI$ salt) – in sharp contrast with the analogous $PY_{14}TFSI$-LiTFSI mixtures. It should be noted that for Li battery applications, it is ideal that the electrolyte not be able to crystallize. Crystallization in the electrolyte of a phase containing the LiX salt results in a precipitous drop in the ionic conductivity and thus battery performance.

References

1. Holzapfel, M.; Jost, C.; Novak, P. *Chem. Commun*. **2004**, *10*, 2098.
2. Holzapfel, M.; Jost, C.; Prodi-Schwab, A.; Krumeich, F.; Wursig, A.; Bupa, H. *Carbon* **2005**, *43*, 1488.
3. Henderson, W. A.; Passerini, S. *Chem. Mater*. **2004**, *16*, 2881.

4. Ishikawa, M.; Sugimoto, T.; Kikuta, M.; Ishiko, E.; Kono, M. *J. Power Sources* **2006**, *162*, 658.

5. Guerfi, A.; Duchesne, S.; Kobayashi, Y.; Vijh, A.; Zaghib, K. *J. Power Sources* **2008**, *175*, 866.

6. Bruba, C. M.; Rocher, N. M.; Frech, R.; Powell, D. R. *J. Phys. Chem. B* **2008**, *112*, 2991.

7. Lerner, H.-W.; Bolte, M. *Acta Crystallogr*. **2003**, *E59*, m625.

8. Matsumoto, K.; Hagiwara, R.; Tamada, O. *Solid State Sciences* **2006**, *8*, 1103.

9. Zhou, Q.; Henderson, W. A.; Appetecchi, G. B.; Montanino, M.; Passerini, S. *J. Phys. Chem. B* **2008**, *112*, 13577.

Chapter 5. Ionic Liquid(1)-Ionic Liquid(2)-Lithium Salt Electrolytes

5.1 Introduction

As noted in Chapter 1, state-of-the-art liquid electrolytes consist of mixtures of aprotic solvents with a lithium salt. The aim is to mix the solvents together to combine their properties with a synergic, beneficial effect. The mixing of ILs for battery electrolytes may also be of interest. For example, the PY_{1R}TFSI-LiTFSI electrolytes are known to have excellent thermal stability, but also have a relatively low ionic conductivity (high viscosity) and tend to solidify into crystalline phases. In contrast, the PY_{1R}FSI-LiFSI mixtures have a higher conductivity (lower viscosity), form an excellent SEI layer on graphite and remained amorphous, but also suffer from a lower thermal stability. As shown in Chapter 4, the addition of LiTFSI to the IM_{10R}TFSI salts improved the thermal stability of the mixtures – such a benefit may also occur for other IL-LiX mixtures. In this chapter, therefore, the properties of PY_{14}TFSI-PY_{13}FSI-LiTFSI and PY_{14}TFSI-PY_{13}FSI-$LiPF_6$ mixtures are explored as electrolytes for Li batteries (Table 5-1 indicates the mole composition of the mixtures).

Table 5-1. Mole composition of (1-x) PY_{14}TFSI-(x) PY_{13}FSI-0.3M LiX mixtures (X = $TFSI^-$ or PF_6^-). The parameters x and (1-x) are the mole fractions of PY_{13}FSI and PY_{14}TFSI, respectively.

PY_{13}FSI		**PY_{14}TFSI**	
Mole fraction	Weight fraction	Mole fraction	Weight fraction
0	0	1	1.00
0.067	0.05	0.933	0.95
0.132	0.10	0.868	0.90
0.255	0.20	0.745	0.80
0.370	0.30	0.630	0.70
0.477	0.40	0.523	0.60
0.578	0.50	0.422	0.50
1	1.00	0	0

$PY_{13}FSI$ exhibits a low viscosity and a low T_m (-9°C) with a high conductivity (6.4 mS cm^{-1}) at room temperature.[1] The electrolyte formed by dissolving LiTFSI in $PY_{13}FSI$ was reported to allow reversible lithium insertion/deinsertion in graphite electrodes.[2] However, $PY_{13}FSI$ shows a lower thermal and electrochemical stability than $PY_{14}TFSI$. $PY_{14}TFSI$ and its mixtures with lithium salts were reported to have a reasonable room temperature ionic conductivity (> 1 mS cm^{-1}) and an overall stability windows in excess of 5.5 V with the cathodic stability limit exceeding the Li/Li^+ plating/stripping potential.[3] $LiPF_6$ was selected because of its wide use and favorable properties as noted in Chapter 1. LiTFSI was also selected for comparison purposes to investigate the effect of the PF_6^- anions (the $TFSI^-$ anion is already present in both ternary mixtures). The lithium salt (i.e., LiTFSI or $LiPF_6$) concentration was fixed at 0.3M based upon preliminary battery cycling test results obtained on carbonaceous anodes.[2]

5.2 (1-x) $PY_{14}TFSI$-(x) $PY_{13}FSI$-0.3M LiX Mixtures (X = $TFSI^-$ or PF_6^-)

Interestingly, there is some significant variation in the DSC heating traces for the same $PY_{13}FSI$-0.3M $LiPF_6$ sample (Fig. 5-1) when various thermal cycling procedures (not shown) are used to crystallize the same sample. The pure $PY_{13}FSI$ salt crystallizes with a T_m of -9°C and

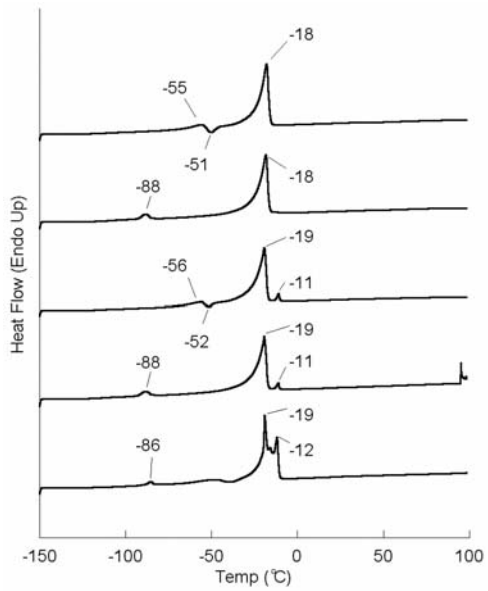

Fig. 5-1. DSC heat traces (5°C min^{-1}) of (1-x) $PY_{14}TFSI$-(x) $PY_{13}FSI$-0.3M $LiPF_6$ (x = 1).

this phase also undergoes solid-solid phase transitions at -83 and -19°C (Chapter 3).[1] Another peak was found for the pure $PY_{13}FSI$ salt at -50°C, but this peak was not reproducible (Chapter 3).[1] One explanation for the inconsistency of the data in Fig. 5-1 is that a small fraction of the sample is sometimes able to crystallize into this crystalline phase (not related to the other phase with its two solid-solid phase transitions) which melts near -55°C and immediately after melting, the liquid recrystallizes (since there is still the other solid crystalline phase present) to the more thermodynamically stable phase. This behavior explains much in Fig. 5-1. It does not, however, account for the new peak observed near -11°C or -12°C. This peak may be due to a new crystalline phase containing both $PY_{13}FSI$ and $LiPF_6$. It is difficult to crystallize this phase, however, and only in the last heating trace is a significant amount of this phase present.

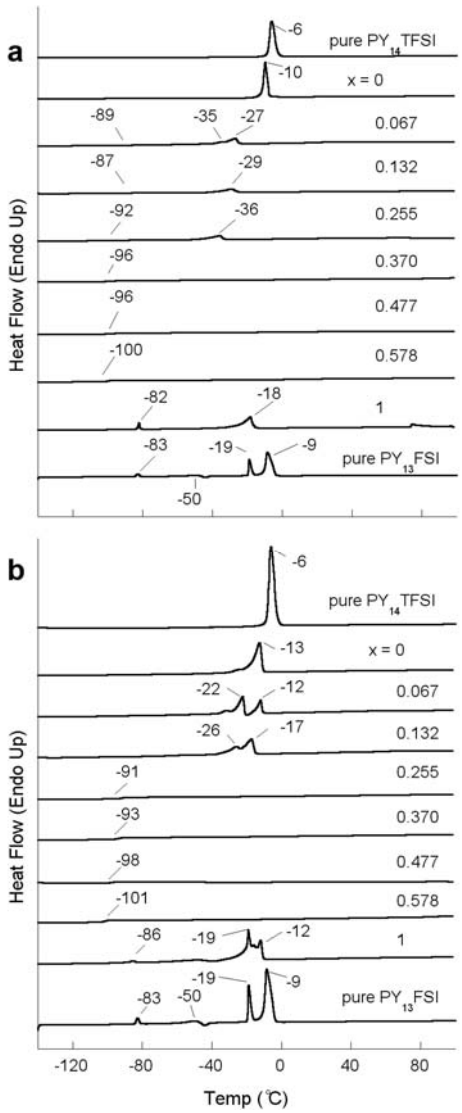

Fig. 5-2. DSC heat traces (5°C min^{-1}) of (1-x) $PY_{14}TFSI$-(x) $PY_{13}FSI$-0.3M LiX mixtures: (a) X = $TFSI^-$ and (b) X = PF_6^-.

Fig. 5-2a shows the DSC heat traces for (1-x) $PY_{14}TFSI$-(x) $PY_{13}FSI$-0.3M LiTFSI mixtures. Pure $PY_{14}TFSI$ has a melting point of -6°C or -7°C.[4] Adding 0.3M LiTFSI (the x = 0 sample)

lowers this melting point to -10°C. As the $PY_{13}FSI$ mole fraction increases (x increases), the amount of $PY_{14}TFSI$ that may be crystallized decreases. The data for the x = 0.067 sample is not in complete agreement with expectations. There is no evidence of one or more higher melting crystalline phase(s) containing the LiTFSI salt despite the presence of only a small amount of $PY_{13}FSI$ and the ready crystallization of such $PY_{14}TFSI$-LiTFSI phases in the absence of $PY_{13}FSI$ (Chapter 4). The x = 0.370, 0.477 and 0.578 samples could not be crystallized despite repeated cycling at low temperature. The T_g tends to decrease with increasing fraction of $PY_{13}FSI$. For the sample containing only $PY_{13}FSI$ (x = 1), some of the pure IL is able to crystallize and the T_m is lower than that of pure $PY_{13}FSI$ due to the presence of the 0.3M LiTFSI salt. It is likely that the T_m and first solid-solid phase transition overlap resulting in the T_m at -18°C. Again, there is no evidence of a new crystalline phase containing the LiTFSI salt. Rather, this salt remains in an amorphous phase with some of the IL (indicated by a small T_g for the sample).

Fig. 5-2b shows the DSC heat traces for (1-x) $PY_{14}TFSI$-(x) $PY_{13}FSI$-0.3M $LiPF_6$

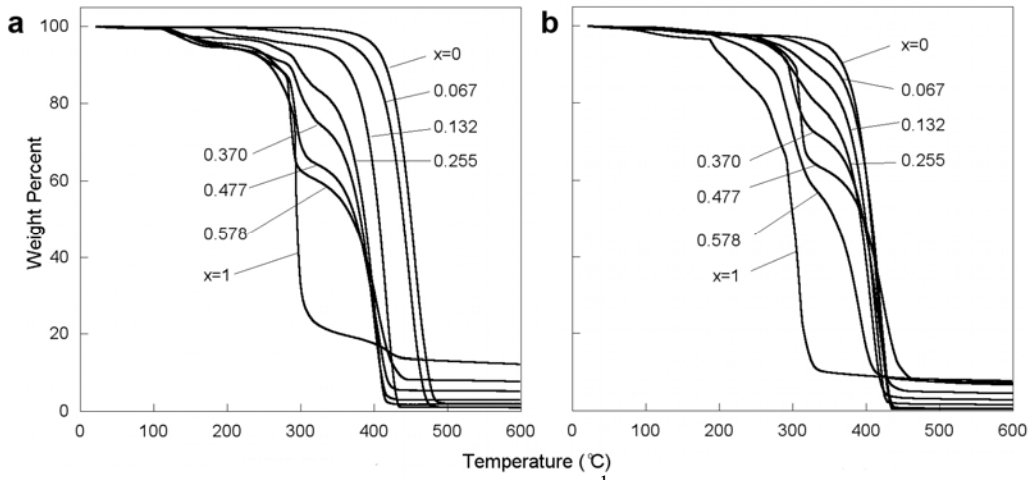

Fig. 5-3. Variable-temperature TGA traces (5°C min^{-1}) of (1-x) $PY_{14}TFSI$-(x) $PY_{13}FSI$-0.3M LiX mixtures: (a) X = $TFSI^-$ and (b) X = PF_6^- (N_2 atmosphere).

mixtures. For the $PY_{14}TFSI$ rich samples (x = 0, 0.067, 0.132), there are clear differences in the melting peaks from what is found for neat $PY_{14}TFSI$ in Chapter 3. These differences may (at least in part) be attributed to the formation of a metastable crystalline phase that may be formed by the pure $PY_{14}TFSI$ salt (Fig. 3-8),[4] as well as the presence of the 0.3M $LiPF_6$. Once again, there is no evidence that a new crystalline phase forms containing the $LiPF_6$ salt for these samples.

Fig. 5-3 indicates that as the $PY_{13}FSI$ mole fraction increases (x increases), the thermal stability of the mixtures decreases (the onset point for mass loss (1 wt%) is about 219-231°C for $PY_{13}FSI$ (Chapter 3) and 350°C for $PY_{14}TFSI$). Note that approximately 8-12 wt% of the sample mass remains after decomposition for the x = 1 samples and no sample mass remains after decomposition for the x = 0 samples, which is in agreement with what was reported in Chapter 3. For the x = 0.255, 0.370, 0.477 and 0.578 samples, a second thermal process beginning near 300°C and finishing near 600°C.

5.3 Discussion

The addition of small amounts of $PY_{13}FSI$ to the $PY_{14}TFSI$-LiTFSI (or $LiPF_6$) electrolytes substantially increases the ionic conductivity (Fig. 5-4)[3] of the mixtures and greatly hinders the ability of the samples to crystallize (Fig. 5-2). The thermal stability of the mixtures is reduced somewhat by the addition of the $PY_{13}FSI$ (Fig. 5-3), but remains quite acceptable for Li battery applications. Thus, the use of mixed ILs for such electrolytes appears to be a very promising approach to optimizing the properties of electrolytes for advanced Li batteries.[2,5]

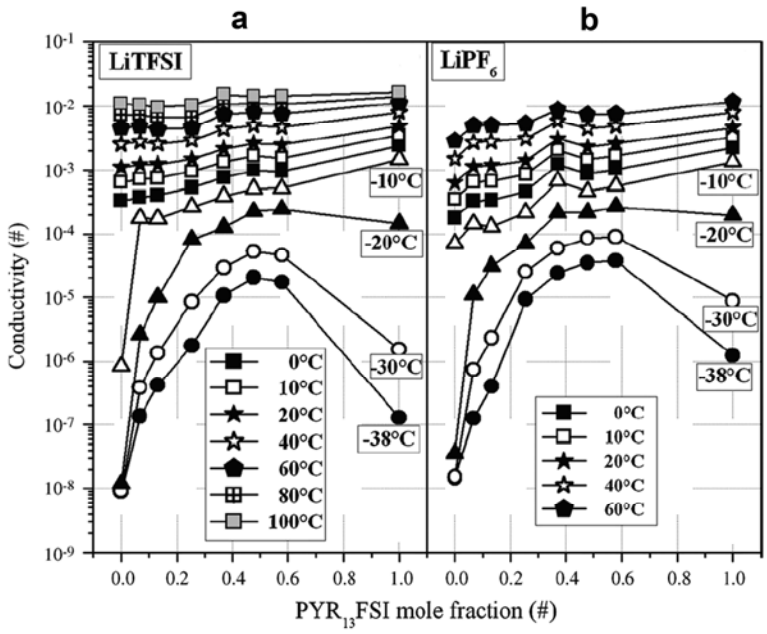

Fig. 5-4. Variable-temperature ionic conductivity of (1-x) $PY_{14}TFSI$-(x) $PY_{13}FSI$-0.3M LiX mixtures: (a) X = $TFSI^-$ and (b) X = PF_6^-.[2]

References

1. Zhou, Q.; Henderson, W. A.; Appetecchi, G. B.; Montanino, M.; Passerini, S. *J. Phys. Chem. B* **2008**, *112*, 13577.
2. Appetecchi, G. B.; Montanino, M. ; Balducci, A.; Lux, S. F. ; Winter, M. ; Passerini, S. *J. Power Sources* **2009**, *192*, 599.
3. Appetecchi, G.B.; Montanino, M.; Zane, D.; Carewska, M.; Alessandrini, F.; Passerini, *S. Electrochim. Acta* **2009**, *54*, 1325.
4. Henderson, W. A.; Passerini, S. *Chem. Mater.* **2004**, *16*, 2881.
5. Lux, S. F.; Schmuck, M.; Appetechi, G. B.; Passerini, S.; Winter, M.; Balducci, A. *J. Power Sources* **2009**, *192*, 606.